

## THE IRON ABUNDANCE IN GALACTIC PLANETARY NEBULAE \*

G. DELGADO-INGLADA AND M. RODRÍGUEZ

Instituto Nacional de Astrofísica, Óptica y Electrónica (INAOE), Apdo Postal 51 y 216, 72000 Puebla, Mexico.

AND

A. MAMPASO AND K. VIIRONEN

Instituto de Astrofísica de Canarias (IAC), C/Vía Láctea s/n, E38205 La Laguna, Tenerife, Spain

*Draft version March 27, 2022*

### ABSTRACT

We constrain the iron abundance in a sample of 33 low-ionization Galactic planetary nebulae (PNe) using [Fe III] lines and correcting for the contribution of higher ionization states with ionization correction factors that take into account uncertainties in the atomic data. We find very low iron abundances in all the objects, suggesting that more than 90% of their iron atoms are condensed onto dust grains. This number is based on the solar iron abundance and implies a lower limit on the dust-to-gas mass ratio, solely due to iron, of  $M_{\text{dust}}/M_{\text{gas}} \geq 1.3 \times 10^{-3}$  for our sample. The depletion factors of different PNe cover about two orders of magnitude, probably reflecting differences in the formation, growth, or destruction of their dust grains. However, we do not find any systematic difference between the gaseous iron abundances calculated for C-rich and O-rich PNe, suggesting similar iron depletion efficiencies in both environments. The iron abundances of our sample PNe are similar to those derived following the same procedure for a group of 10 Galactic H II regions. These high depletion factors argue for high depletion efficiencies of refractory elements onto dust grains both in molecular clouds and asymptotic giant branch stars, and low dust destruction efficiencies both in interstellar and circumstellar ionized gas.

*Subject headings:* planetary nebulae: general – ISM: abundances – dust, extinction

### 1. INTRODUCTION

The progenitors of planetary nebulae (PNe), asymptotic giant branch (AGB) stars, have atmospheres particularly favorable for grain formation, and are considered the most efficient source of circumstellar dust (Whittet 2003; Ferrarotti & Gail 2006, and references therein). However, it is not clear yet how much dust do PNe have and whether this dust is destroyed or modified during their lifetime. Pottasch et al. (1984) and Lenzuni et al. (1989) studied PNe with *IRAS* data and found that their derived dust-to-gas mass ratios decreased with nebular radius (which they used as a proxy for nebular age). However, these results strongly depend on the poorly known distances to the studied PNe, and were called into question by Stasińska & Szczerba (1999), who derived dust-to-gas ratios using distance-independent quantities and found no correlation with the surface brightness in  $H\beta$ , their proxy for nebular age. Stasińska & Szczerba concluded that there is no evidence for a decrease in the dust-to-gas mass ratio as PNe evolve, but since there are many uncertainties involved, the issue is far from being settled.

As an alternative to dust-to-gas mass ratios derived from infrared emission, one might consider studying dust through element depletions. Elements such as Al, Ca, Si, Ni and Fe have abundances in the interstellar medium (ISM) much lower than solar (Morton et al. 1973; Morton 1974), and this is generally interpreted as due to their depletion in dust grains. The differences in

depletion factors found in different environments give important clues on the nature of the formation and destruction mechanisms for dust grains in the ISM (see, e.g., Whittet 2003), and the depletion factors in PNe can provide clues on the mechanisms that operate in ionized gas. To study the sensitivity of depletions to environment one must choose an element that is mostly condensed into dust grains, like those mentioned above, since in that case the destruction of a small quantity of dust will translate into a measurable increase of the element abundance in the gas. However, the abundances of these elements are usually difficult to measure in ionized gas due to the lack of suitable emission lines or atomic data, and due to the highly uncertain corrections for unobserved ions. These problems, combined with the wide spread in the degrees of ionization, and hence of ionization states, found in PNe, imply that the depletion factors derived so far for PNe use different ions and ionization correction factors (ICFs) and are not only uncertain, but also difficult to compare between them. The published values for the abundances of refractory elements in PNe cover the ranges: 1/6–1/300 the solar abundance for Ca, 1/2–1/350 for Al, 1/3–1/300 for Fe, near solar to 1/10 solar for Mg, and near solar to 1/20 solar for Si (Shields 1975; Garstang et al. 1978; Shields 1978; Péquignot & Stasińska 1980; Aller et al. 1981; Shields et al. 1981; Aller & Czyzak 1983; Beckwith et al. 1984; Pwa et al. 1986; Clegg et al. 1987a,b; Middlemass 1990; Keyes et al. 1990; Kingdon et al. 1995; Pottasch & Beintema 1999; Perinotto et al. 1999; Casassus et al. 2000; Pottasch et al. 2001; Pottasch et al. 2002, 2003; Liu et al. 2004a; Pottasch & Surendiranath 2005;

\*PARTLY BASED ON OBSERVATIONS MADE WITH THE 2.1-M TELESCOPE AT OBSERVATORIO ASTRONÓMICO NACIONAL, SAN PEDRO MÁRTIR, MEXICO.

Electronic address: gloria@inaoep.mx, mrodri@inaoep.mx, amr@iac.es, kerttu@iac.es

Sterling et al. 2005; Georgiev et al. 2006; Likkell et al. 2006; Pottasch & Surendiranath 2007; Pottasch et al. 2007, 2008).

The problem with the determination of depletion factors in ionized gas is somewhat alleviated in the case of H II regions, where the range of degrees of ionization is much smaller. However, dust grains in PNe and H II regions are likely to have very different characteristics. The dust grains present in PNe formed in the cool atmospheres of the progenitor stars, whereas those grains now present in H II regions were located before in the associated molecular clouds and can be considered processed interstellar dust grains. Therefore, it is important to perform a homogeneous study of depletion factors in a sample of PNe, and especially so if the results can also be compared with those found in H II regions. Differences in depletion factors can provide much information on the efficiency of dust formation and destruction processes.

Of all the refractory elements we mentioned above, Fe has the strongest lines in the visible range of the spectrum. Furthermore, since most of the Fe atoms are condensed into dust grains and since the cosmic abundance of Fe is relatively high, this element is an important contributor to the mass of refractory dust grains (Sofia et al. 1994), and the Fe gaseous abundance will probably reflect the abundance of refractory elements in dust. These reasons make Fe a good choice to study depletion factors in ionized gas.

The comparison between the results derived in PNe and H II regions will be more meaningful if the sample of PNe is restricted to objects with a low degree of ionization, because in that case the same ions need to be considered in the abundance determination for both types of objects. In H II regions, Fe will be mostly found in three ionization states:  $\text{Fe}^+$ ,  $\text{Fe}^{++}$ , and  $\text{Fe}^{+3}$ .  $\text{Fe}^+$  has a low ionization potential and its contribution to the total abundance is often negligible (Rodríguez 2002). On the other hand, [Fe IV] lines are weak and more difficult to measure than [Fe III] lines. Hence, Fe abundances are usually calculated from  $\text{Fe}^{++}$  abundances and an ICF derived from photoionization models. However, for the handful of objects in which [Fe IV] lines have been measured, this ICF can be compared with that implied by the derived  $\text{Fe}^{+3}$  abundances, and a discrepancy has been found between them (Rodríguez 2003, and references therein). Rodríguez & Rubin (2005) determined what changes in all the atomic data involved in the calculations would explain this discrepancy: (1) a decrease in the collision strengths for  $\text{Fe}^{+3}$  by factors of 2–3, (2) an increase in the collision strengths for  $\text{Fe}^{++}$  by factors of 2–3, or (3) an increase in the total recombination coefficient or the rate of the charge-exchange reaction with  $\text{H}^0$  for  $\text{Fe}^{+3}$  by a factor of  $\sim 10$ . Rodríguez & Rubin (2005) argued that the three explanations are equally plausible, and derived two different ICFs:

$$\frac{\text{Fe}}{\text{O}} = 0.9 \left( \frac{\text{O}^+}{\text{O}^{++}} \right)^{0.08} \frac{\text{Fe}^{++}}{\text{O}^+} \quad (1)$$

$$\frac{\text{Fe}}{\text{O}} = 1.1 \left( \frac{\text{O}^+}{\text{O}^{++}} \right)^{0.58} \frac{\text{Fe}^{++}}{\text{O}^+} \quad (2)$$

Equation (1) is based on photoionization models that use the state-of-the-art values for the atomic data rele-

vant to the problem, and Equation (2) is derived from those objects with measurements of [Fe IV] lines (see Rodríguez & Rubin 2005). Equation (2) should be replaced by

$$\frac{\text{Fe}}{\text{O}} = \frac{\text{Fe}^+ + \text{Fe}^{++}}{\text{O}^+} \quad (3)$$

for those objects with  $\log(\text{O}^+/\text{O}^{++}) \geq -0.1$ , since  $\text{Fe}^{++}$  and  $\text{O}^+$  will then dominate the total abundances of Fe and O. If the discrepancy were completely due to errors in the collision strengths for  $\text{Fe}^{+3}$ , good values of the Fe abundance could be obtained from the ICF of Equation (1). If the collision strengths for  $\text{Fe}^{++}$  were the ones to blame, the correct abundance would be the previous value lowered by  $\sim 0.3$  dex. Finally, if the models predictions were wrong – due to errors in the total recombination coefficient or the rate of the charge-exchange reaction – the ICF of equation (2) would give the best values of the Fe abundance. The discrepancy is probably due to some combination of the aforementioned causes, therefore the errors required in any of the atomic data are likely to be lower than those considered above, and the values of the Fe abundance will consequently be intermediate between the extreme values obtained with the ICF scheme described above.

The three ionization correction schemes give values of the Fe abundance that can be similar or differ by more than a factor of 10, but since these schemes involve drastic changes in the atomic data involved in the abundance calculation, the extreme values of the Fe abundance implied by them can be used to constrain the true values of the Fe abundances in the gas. Rodríguez & Rubin (2005) followed this procedure and found that the two Galactic H II regions and the four Galactic PNe of their sample have less than 5% of their Fe atoms in the gas phase. In this paper, we apply this procedure to constrain the Fe abundances in a sample of 33 low-ionization Galactic PNe, and compare the results with the values obtained for 10 Galactic H II regions.

## 2. THE SAMPLE

In order to perform the analysis described above, we need to select a sample of low-ionization PNe where  $\text{Fe}^+$ ,  $\text{Fe}^{++}$ , and  $\text{Fe}^{+3}$  (the latter with ionization potential  $\text{IP} = 54.8$  eV) are the main ionization states of iron and  $\text{O}^+$ ,  $\text{O}^{++}$  (the latter with  $\text{IP} = 54.9$  eV) are the main ionization states of oxygen. We considered a group of PNe that have determinations of the  $\text{O}^{+3}$  abundance (Liu et al. 2004a; Tsamis et al. 2003), and found that those with  $I(\text{He II } \lambda 4686)/I(\text{H}\beta) \lesssim 0.3$  have less than 10% of their O abundance in this ionization state. Hence, we established this as the condition that our sample PNe should satisfy.

The initial sample consists of 28 low-ionization PNe, 23 of them selected from the literature because their published spectra have all the lines we need to calculate physical conditions and the  $\text{Fe}^{++}$  and O ionic abundances. Three of these PNe do not have measurements of [Fe III] lines, but do have measurements of weak, nearby recombination lines which can be used to calculate upper limits to the  $\text{Fe}^{++}$  and Fe abundances. The other 5 PNe of the sample were observed in the 2.1-m telescope at Observatorio Astronómico Nacional (San Pedro Mártir, Mexico).

Our initial sample does not contain PNe with high electron densities ( $n_e \gtrsim 25,000 \text{ cm}^{-3}$ ) because it is difficult to obtain good estimates of the physical conditions in these objects. However, we have included 5 additional PNe with  $n_e > 25,000 \text{ cm}^{-3}$ , and performed a special analysis, as described in Section 6.

### 3. OBSERVATIONS AND DATA REDUCTION

Long-slit spectra covering the wavelength ranges  $\lambda\lambda 3600\text{--}5700$  and  $\lambda\lambda 5350\text{--}7500$  were obtained with the Boller & Chivens spectrograph and the SITe3 CCD detector in the 2.1-m telescope at Observatorio Astronómico Nacional (San Pedro Mártir, Mexico). The spectral ranges were covered with a spectral resolution of  $\sim 4 \text{ \AA}$  using a  $600 \text{ lines mm}^{-1}$  grating at two different angles, and a slit width of  $2''$ . The observed objects, the positions and position angles (P.A.) of the slit, and the exposure times are listed in Table 1. The slit was positioned at the center of the nebulae with the exception of JnEr 1, where the slit was placed at the NW condensation. Bias frames, twilight and tungsten flat-field exposures, wavelength calibrations, and exposures of standard stars were taken each night. The angular diameters of IC 4593, NGC 2392, and NGC 6210 are smaller than the slit length and suitable sky windows could be selected on either side of the nebular emission. For NGC 3587 and JnEr 1, sky spectra were obtained near the objects after the nebular exposures. The spectra were reduced using the IRAF<sup>1</sup> reduction package and following the standard procedures for long-slit reductions. After the bias subtraction, flat-field correction, and wavelength calibration, the images were flux calibrated with the standard stars Feige 34, Feige 56 and G191B2B. We subtracted the sky (after scaling it by factors of 0.5–1.5 to obtain the best cancelation in those cases where the sky spectra were observed separately), and removed cosmic rays by the combination of different exposures. Finally, one-dimensional spectra were extracted.

Line intensities were measured by integrating between two given limits above a continuum around each line estimated by eye. In the cases of line blending, a multiple Gaussian profile-fitting procedure was applied to obtain the intensity of each individual line. These measurements were made with the SPLOT routine of the IRAF package. The line intensities were first normalized to the brightest H I line appearing in the same spectral range: H $\beta$  for the blue range and H $\alpha$  for the red range. These line ratios were corrected for extinction using the extinction law of Cardelli et al. (1989) with a total to selective extinction ratio  $R_V = A(V)/E(B - V) = 3.1$ , the mean value for the diffuse interstellar medium. The logarithmic extinction  $c(\text{H}\beta)$  was calculated from the comparison between the observed and theoretical ratio  $I(\text{H}\beta)/I(\text{H}\gamma)$  for typical physical conditions (Storey & Hummer 1995):  $T_e = 10,000 \text{ K}$  and  $n_e = 100, 5000$  or  $10,000 \text{ cm}^{-3}$  depending on the PN. Dereddened intensities were obtained by multiplying the observed intensity ratios by the factor  $10^{c(\text{H}\beta) f(\lambda)}$ , where  $f(\lambda)$  comes from the extinction law. Columns 1 and 2 in Table 2 show the laboratory and

observed wavelengths, Column 3 shows the line identifications, and Columns 4 and 5 contain the observed  $[I_{\text{ob}}(\lambda)]$  and dereddened  $[I(\lambda)]$  line intensities, normalized with respect to  $I(\text{H}\beta) = 100$ . The intensities of lines in the red range were normalized with respect to  $I(\text{H}\beta)$  using the theoretical value of the ratio  $I(\text{H}\alpha)/I(\text{H}\beta)$  and the value derived for  $c(\text{H}\beta)$ . The logarithmic extinction  $c(\text{H}\beta)$ , the observed and dereddened intensity of H $\beta$ , and the extraction window are also given for each object in Table 2.

The errors in the line intensities were obtained by adding quadratically: (1) the error due to the flux calibration (4% in the blue range and 3% in the red range) derived from the standard deviation in the calibration curves of the standard stars; (2) the statistical errors associated with the measurement of the line intensities, which have been calculated using  $\sigma_1 = \sigma_c \sqrt{N + EW/\Delta}$  (Pérez-Montero & Díaz 2003), where  $\sigma_1$  is the error in the observed line intensity,  $\sigma_c$  represents the standard deviation in a box near the measured emission line and stands for the error in the continuum placement,  $N$  is the number of pixels used in the measurement of the line intensity,  $EW$  is the line equivalent width, and  $\Delta$  is the wavelength dispersion in  $\text{\AA pixel}^{-1}$ ; and (3) the error associated with the extinction correction.

Figures 1 and 2 show the  $\lambda\lambda 4600\text{--}5000$  spectral region of the observed objects, where most of the [Fe III] lines are located.

### 4. PHYSICAL CONDITIONS AND IONIC ABUNDANCES

We calculated physical conditions and ionic abundances for the five PNe we observed, and recalculated them from the line intensities available in the literature for the rest of the PNe in our sample. We used the diagnostic line ratios  $[\text{N II}] \lambda 5755 / (\lambda 6548 + \lambda 6584)$  and  $[\text{O III}] \lambda 4363 / (\lambda 4959 + \lambda 5007)$  to derive the electron temperatures ( $T_e$ ) of the low and high-ionization regions, respectively. The adopted electron density for each PN is the weighted mean of the  $n_e$  values obtained from the available line ratios of the three diagnostics we used:  $[\text{S II}] \lambda 6716 / \lambda 6731$ ,  $[\text{Cl III}] \lambda 5518 / \lambda 5538$  and  $[\text{Ar IV}] \lambda 4711 / \lambda 4740$ . Table 3 shows the values of  $T_e$  and  $n_e$  we derived for each PN of the sample, and the references for the line intensities. The maximum differences between the physical conditions we obtained and the ones presented in the literature are of about 20% for  $T_e$  and 40% for  $n_e$ ; these differences are mostly due to the use of different atomic data.

The [N II]  $\lambda 5755$  line can be affected by recombination excitation, and Liu et al. (2000) derived an expression that can be used to correct for this effect the value of  $T_e([\text{N II}])$ . We checked and found that the effect of this correction in the total abundances of O and Fe is not important for the PNe in our sample: if we had considered the contribution of recombination excitation, the derived total abundances would be consistent within the errors with those presented here. For this reason, and because the value of the correction is somewhat uncertain, we did not take this effect into account.

We used the values of  $T_e([\text{N II}])$  to derive the  $\text{O}^+$  and  $\text{Fe}^{++}$  abundances, and  $T_e([\text{O III}])$  for  $\text{He}^+$ ,  $\text{He}^{++}$ , and  $\text{O}^{++}$ . We calculated the  $\text{He}^+$  and  $\text{He}^{++}$  abundances in order to estimate the contribution to the total O abundance of ions of higher degree of ionization than  $\text{O}^{++}$

<sup>1</sup> IRAF is distributed by the National Optical Astronomy Observatories, which are operated by the Association of Universities for Research in Astronomy, Inc., under cooperative agreement with the National Science Foundation.

TABLE 1  
JOURNAL OF OBSERVATIONS

Object	$\alpha$ (2000) (hh mm ss)	$\delta$ (2000) ( $^{\circ}$ ' ")	P.A. ( $^{\circ}$ )	Date <sup>a</sup>	Exposure times <sup>a</sup> (s)
IC 4593	16 11 44.54	+12 04 17.06	0	2006 Jan 28, 29	10, 3 $\times$ 30, 60, 29 $\times$ 120
JnEr 1	07 58 19.00	+53 25 17.00	90	2006 Jan 28, 29	30, 4 $\times$ 40, 2 $\times$ 100, 5 $\times$ 300
NGC 2392	07 29 10.77	+20 54 42.49	65	2006 Jan 27	4 $\times$ 1200
NGC 3587	11 14 47.73	+55 01 08.50	55	2007 Jan 22, 24	6 $\times$ 60, 17 $\times$ 120
NGC 6210	16 44 29.49	+23 47 59.68	90	2007 Jan 23	60, 12 $\times$ 120
				2006 Jan 26	5 $\times$ 1200
				2006 Jan 25	5 $\times$ 1200
				2006 Jan 28, 29	3 $\times$ 10, 20 $\times$ 60
				2006 Jan 27	3, 19 $\times$ 15

<sup>a</sup> The first entry corresponds to the blue range  $\lambda\lambda 3600\text{--}5700$  and the second one corresponds to the red range  $\lambda\lambda 5350\text{--}7500$ .

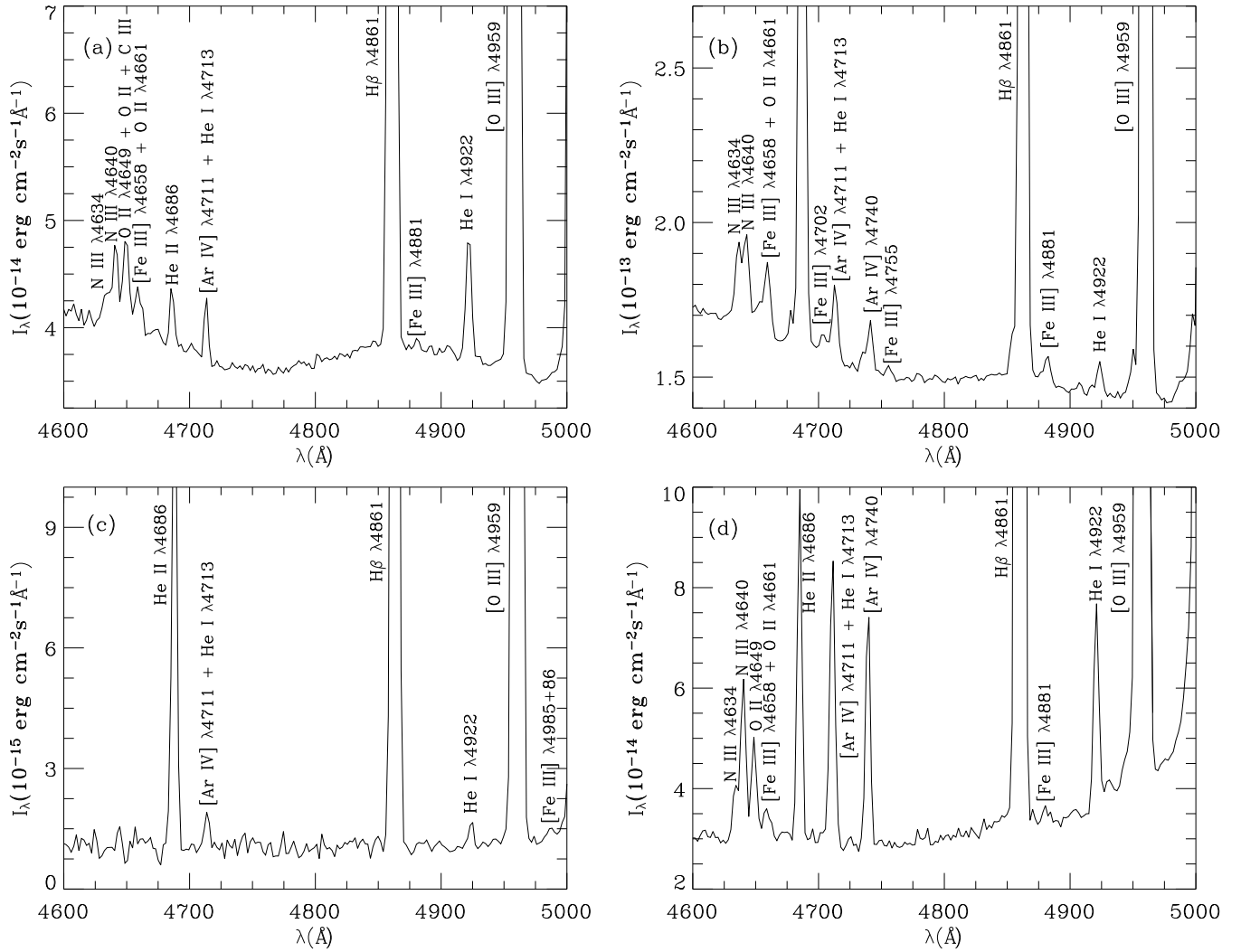


FIG. 1.— Part of the blue spectra of (a) IC 4593, (b) NGC 2392, (c) NGC 3587, and (d) NGC 6210 showing the region where we find most of the [Fe III] lines.

TABLE 2  
OBSERVED AND REDDENING-CORRECTED LINE  
RATIOS WITH RESPECT TO  $I(\text{H}\beta) = 100$ .

$\lambda(\text{\AA})$	$\lambda_{\text{ob}}(\text{\AA})$	Ion	$I_{\text{ob}}(\lambda)$	$I(\lambda)$
IC 4593				
3703.85	3705.02	H 16	1.50±0.45	1.79±0.58
3705.02	*	He I	*	*
3711.97	3712.73	H 15	1.21±0.11	1.45±0.22
3726.03	3727.28	[O II]	42.07±2.4	50.3±6.6
3728.82	*	[O II]	*	*
3770.63	3770.79	H 11	3.64±0.23	4.33±0.57
3797.90	3797.87	H 10	2.85±0.18	3.38±0.44
3819.61	3819.72	He I	1.01±0.10	1.20±0.18
3835.39	3835.63	H 9	4.50±0.27	5.31±0.66
3868.75	3869.01	[Ne III]	27.7±1.6	32.6±4.0
3888.65	3889.07	He I	16.90±0.96	19.8±2.4
3889.05	*	H 8	*	*
3967.46	3969.15	[Ne III]	21.8±1.2	25.2±2.9
3970.07	*	H 7	*	*
4009.22	4009.32	He I	0.333±0.089	0.38±0.11
4026.08	4026.58	N II	1.47±0.11	1.69±0.20
4026.21	*	He I	*	*
4101.74	4101.95	H 6	22.4±1.3	25.4±2.6
4132.80	4133.61	O II	0.140±0.082	0.158±0.094
4143.76	4144.24	He I	0.339±0.094	0.38±0.11
4153.30	4154.46	O II	0.295±0.093	0.33±0.11
4156.53	*	O II	*	*
4267.15	4267.65	C II	0.416±0.095	0.46±0.11
4340.47	4340.71	H 5	43.0±2.4	46.9±3.8
4363.21	4363.76	[O III]	1.83±0.14	1.99±0.19
4387.93	4388.48	He I	0.542±0.088	0.59±0.10
4471.49	4471.69	He I	4.74±0.27	5.06±0.36
4634.14	4634.90	N III	0.713±0.057	0.740±0.061
4640.64	4641.40	O II	0.776±0.059	0.804±0.064
4641.81	*	O II	*	*
4641.84	*	N III	*	*
4643.31	*	N II	*	*
4647.42	4648.18	C III	0.739±0.058	0.764±0.062
4649.13	*	O II	*	*
4650.25	4651.26	C III	0.477±0.048	0.493±0.051
4650.84	*	O II	*	*
4658.10	4659.02	[Fe III]	0.692±0.056	0.714±0.060
4661.63	4662.44	O II	0.054±0.039	0.056±0.040
4685.68	4685.03	He II	0.418±0.052	0.430±0.054
4701.62	4702.22	[Fe III]	0.124±0.042	0.127±0.043
4711.37	4711.37	[Ar IV]	0.511±0.049	0.523±0.051
4713.17	*	He I	*	*
4861.33	4861.27	H 4	100.0±5.7	100.0±5.7
4881.11	4880.92	[Fe III]	0.118±0.039	0.118±0.039
4890.86	4889.70	[Fe II]	0.058±0.036	0.057±0.036
	4891.72	O II	*	*
4906.83	4905.34	[Fe II]	0.104±0.047	0.103±0.046
	4907.03	O II	*	*
4921.93	4922.00	He I	1.444±0.097	1.431±0.096
4958.91	4958.77	[O III]	197±11	194±11
5006.84	5006.67	[O III]	555±31	544±32
5015.68	5015.99	He I	1.043±0.066	1.020±0.066
5047.74	5047.65	He I	0.184±0.031	0.179±0.031
5191.82	5191.88	[Ar III]	0.086±0.032	0.072±0.030
5270.40	5268.77	[Fe III]	0.338±0.047	0.320±0.046
5517.66	5516.59	[Cl III]	0.416±0.049	0.384±0.048
5537.60	5536.91	[Cl III]	0.340±0.044	0.313±0.044
5666.63	5666.31	N II	0.110±0.032	0.108±0.032
5754.60	5754.84	[N II]	0.146±0.035	0.143±0.034
5875.66	5876.27	He I	15.86±0.80	15.30±0.84
6300.34	6299.44	[O I]	0.146±0.047	0.137±0.044
6312.10	6312.66	[S II]	0.816±0.067	0.761±0.060
6548.10	6548.62	[N II]	3.91±0.20	3.58±0.15
6562.77	6563.02	H 3	100.0±4.2	286±12
6583.50	6583.67	[N II]	11.39±0.57	10.41±0.44
6678.16	6678.26	He I	4.59±0.23	4.17±0.18
6716.44	6716.58	[S II]	0.667±0.041	0.604±0.034
6730.82	6730.96	[S II]	0.930±0.052	0.841±0.042
7065.25	7064.63	He I	4.48±0.23	3.95±0.20
7135.80	7135.10	[Ar III]	10.78±0.54	9.47±0.48
7280.76	7280.76	He I	0.848±0.049	0.737±0.046

TABLE 2  
-continued

$\lambda(\text{\AA})$	$\lambda_{\text{ob}}(\text{\AA})$	Ion	$I_{\text{ob}}(\lambda)$	$I(\lambda)$
IC 4593 (cont.)				
7318.92	7319.09	[O II]	1.539±0.082	1.333±0.079
7329.67	7329.85	[O II]	1.201±0.065	1.040±0.063
c(H $\beta$ ) = 0.24 ± 0.16				
$I_{\text{ob}}(\text{H}\beta) = 4.462 \times 10^{-12} \text{ erg cm}^{-2} \text{ s}^{-1}$				
$I(\text{H}\beta) = 7.754 \times 10^{-12} \text{ erg cm}^{-2} \text{ s}^{-1}$				
Extraction window = 2'' × 15''				
JnEr 1				
3711.97	3710.54	H 15	117±25	151±48
3726.03	3727.29	[O II]	608±54	783±193
3728.82	*	[O II]	*	*
3734.37	3734.05	H 13	41±13	53±21
3756.10	3758.73	He I	28.7±7.7	37±13
3797.90	3798.16	H 10	29.8±8.8	38±14
3868.75	3868.09	[Ne III]	98±13	122±30
3967.46	3967.98	[Ne III]	39±11	48±16
3970.07	*	H 7	*	*
4083.90	4083.61	O II	16.6±3.8	20.0±5.6
4085.11	*	O II	*	*
4101.74	4102.56	H 6	34.0±5.4	40.7±9.3
4340.63	4340.60	H 5	41.4±3.4	46.8±6.5
4363.21	4361.65	[O III]	5.1±1.3	5.7±1.6
4471.50	4471.77	He I	9.7±1.8	10.6±2.2
4487.72	4487.61	O II	2.1±1.2	2.3±1.3
4488.20	*	O II	*	*
4489.49	*	O II	*	*
4609.44	4610.27	O II	2.81±0.67	2.98±0.73
4610.20	*	O II	*	*
4658.10	4659.44	[Fe III]	2.34±0.75	2.45±0.79
4661.63	*	O II	*	*
4685.68	4685.80	He II	20.1±1.6	20.9±1.8
4711.37	4713.69	He I	2.23±0.84	2.31±0.87
4713.17	*	[Ar IV]	*	*
4740.17	4740.05	[Ar IV]	5.4±1.1	5.6±1.1
4861.33	4861.00	H 4	100.0±6.3	100.0±6.3
4958.91	4958.51	[O III]	159.9±9.7	157±10
5006.84	5006.36	[O III]	456±27	443±29
5197.90	5198.36	[N I]	11.60±0.89	10.9±1.0
5200.26	*	[N I]	*	*
5411.52	5411.90	He II	2.88±0.54	3.22±0.72
5537.60	5537.27	[Cl III]	0.75±0.37	0.66±0.33
5754.60	5754.17	[N II]	8.98±0.88	9.6±1.2
5875.66	5875.66	He II	27.0±1.7	28.3±2.5
6300.34	6302.66	[O I]	25.9±2.0	26.0±2.0
6312.10	6309.84	[S III]	5.98±1.0	6.0±1.0
6310.80	*	He II	*	*
6363.78	6366.14	[O II]	9.3±1.1	9.2±1.1
6548.10	6547.97	[N II]	222±12	217±9.7
6562.77	6562.80	H 3	294±16	286±13
6583.50	6583.36	[N II]	682±37	664±29
6678.16	6678.16	He I	7.82±0.88	7.54±0.82
6716.44	6716.49	[S II]	28.5±1.8	27.3±1.6
6730.82	6731.01	[S II]	22.5±1.6	21.6±1.4
7065.25	7063.95	He I	4.4±1.1	4.1±1.0
7135.64	7135.02	[Ar III]	23±2.2	21.3±2.3
7319.99	7318.65	[O III]	23±11	21.1±9.6
7330.73	7331.29	[O III]	12.9±8.9	11.6±8.0
c(H $\beta$ ) = 0.34 ± 0.31				
$I_{\text{ob}}(\text{H}\beta) = 3.663 \times 10^{-14} \text{ erg cm}^{-2} \text{ s}^{-1}$				
$I(\text{H}\beta) = 8.014 \times 10^{-14} \text{ erg cm}^{-2} \text{ s}^{-1}$				
Extraction window = 2'' × 42''				
NGC 2392				
3726.03	3728.98	[O II]	105.8±6.1	135±28
3728.82	*	[O II]	*	*
3835.39	3837.09	H 9	2.31±0.19	2.90±0.59
3868.75	3870.42	[Ne III]	95.3±5.4	119±22
3888.65	3890.44	He I	13.69±0.80	17.0±3.2
3889.05	*	H 8	*	*

TABLE 2  
–continued

$\lambda(\text{\AA})$	$\lambda_{\text{ob}}(\text{\AA})$	Ion	$I_{\text{ob}}(\lambda)$	$I(\lambda)$
NGC 2392 (cont.)				
3967.46	3969.71	[Ne III]	34.3±2.0	42.06±7.4
3970.07	*	H 7	*	*
4068.60	4070.93	[S II]	1.89±0.18	2.27±0.40
4101.74	4103.09	H 6	21.3±1.2	25.3±3.9
4120.84	4119.10	He I	1.29±0.19	1.53±0.31
4121.46	*	O II	*	*
4143.76	4145.07	He I	0.72±0.17	0.84±0.23
4227.74	4229.36	N II	0.38±0.14	0.44±0.17
4340.47	4341.71	H 5	41.6±2.4	46.9±5.3
4363.21	4364.54	[O III]	16.74±0.95	18.8±2.0
4465.41	4467.08	O II	0.772±0.077	0.84±0.10
4466.42	*	O II	*	*
4471.49	4472.94	He I	2.70±0.17	2.95±0.28
4518.15	4516.85	N III	1.51±0.11	1.63±0.16
4638.86	4637.25	N III	3.55±0.21	3.72±0.26
4641.81	4643.39	O II	2.02±0.13	2.12±0.16
4641.84	*	N III	*	*
4643.08	*	N II	*	*
4658.10	4659.23	[Fe III]	2.33±0.15	2.44±0.18
4676.24	4678.39	O II	0.650±0.070	0.676±0.076
4685.68	4686.99	He II	30.8±1.8	32.0±2.1
4701.62	4703.67	[Fe III]	0.515±0.069	0.533±0.073
4711.37	4713.07	[Ar IV]	1.96±0.13	2.03±0.15
4713.17	*	He I	*	*
4740.17	4740.81	[Ar III]	1.30±0.097	1.33±0.10
4754.72	4756.13	[Fe III]	0.337±0.062	0.335±0.064
4861.33	4862.53	H 4	100.0±5.7	100.0±5.7
4881.11	4882.58	[Fe III]	0.703±0.072	0.700±0.071
4906.83	4907.85	O II	0.195±0.052	0.194±0.052
4921.93	4923.67	He I	0.240±0.057	0.862±0.080
4958.91	4960.14	[O III]	358±20	351±21
5006.84	5008.17	[O III]	1065±60	1035±63
5159.44	5159.12	[Fe II]	0.219±0.030	0.207±0.030
5270.40	5270.83	[Fe III]	1.209±0.076	1.123±0.098
5411.52	5412.22	He I	1.95±0.12	1.77±0.17
5517.66	5518.18	[Cl III]	0.789±0.056	0.71±0.08
5537.60	5538.29	[Cl III]	0.662±0.049	0.59±0.070
5679.56	5680.88	N II	0.128±0.024	0.11±0.24
5754.60	5757.09	[N II]	0.770±0.095	2.24±0.19
5875.66	5878.32	He I	9.46±0.48	11.80±0.86
6300.34	6303.56	[O I]	1.07±0.19	1.27±0.23
6312.10	6314.86	[S III]	2.78±0.14	3.32±0.16
6363.78	6367.24	[O I]	0.447±0.040	0.53±0.46
6548.10	6551.06	[N II]	27.2±1.4	31.6±1.3
6562.77	6565.53	H 3	246±12	286±12
6583.50	6586.40	[N II]	78±3.9	90.8±3.8
6678.16	6680.96	He I	2.65±0.14	3.05±0.14
6716.44	6719.44	[S II]	6.02±0.30	6.88±0.31
6730.82	6733.80	[S II]	8.73±0.44	9.96±0.45
7065.25	7067.87	He I	2.16±0.12	2.38±0.15
7135.80	7138.20	[Ar III]	11.41±0.57	12.50±0.80
7281.35	7284.05	He I	0.54±0.047	0.582±0.060
7319.99	7322.22	[O II]	3.56±0.18	3.83±0.29
7330.73	7333.22	[O II]	2.83±0.15	3.04±0.24

$c(\text{H}\beta) = 0.33 \pm 0.27$

$I_{\text{ob}}(\text{H}\beta) = 6.458 \times 10^{-12} \text{ erg cm}^{-2} \text{ s}^{-1}$

$I(\text{H}\beta) = 1.381 \times 10^{-12}$

Extraction window = 2'' × 14''

NGC 3587

3711.97	3710.54	H 15	117±25	151±48
3726.03	3727.29	[O II]	608±54	783±193
3728.82	*	[O II]	*	*
3734.37	3734.05	H 13	41±13	53±21
3756.10	3758.73	He I	28.7±7.7	37±13
3797.90	3798.16	H 10	29.8±8.8	38±14
3868.75	3868.09	[Ne III]	98±13	122±30
3967.46	3967.98	[Ne III]	39±11	48±16
3970.07	*	H 7	*	*
4083.90	4083.61	O II	16.6±3.8	20.0±5.6
4085.11	*	O II	*	*

TABLE 2  
–continued

$\lambda(\text{\AA})$	$\lambda_{\text{ob}}(\text{\AA})$	Ion	$I_{\text{ob}}(\lambda)$	$I(\lambda)$
NGC 3587 (cont.)				
4101.74	4102.56	H 6	34.0±5.4	40.7±9.3
4340.63	4340.60	H 5	41.4±3.4	46.8±6.5
4363.21	4365.27	[O III]	7.99±0.55	8.45±0.96
4471.50	4473.72	He I	4.91±0.41	5.12±0.55
4514.90	4515.34	[Fe II]	0.69±0.17	0.71±0.18
4514.86	*	N III	*	*
4641.81	4644.15	O II	0.65±0.18	0.67±0.19
4641.84	*	N III	*	*
4643.08	*	N II	*	*
4685.68	4687.92	He II	16.4±1.0	16.7±1.2
4701.62	4702.56	[Fe III]	0.14±0.16	0.14±0.16
4711.37	4713.86	[Ar IV]	1.13±0.22	1.15±0.23
4713.17	*	He I	*	*
4740.17	4743.35	[Ar IV]	0.34±0.18	0.35±0.18
4861.33	4863.37	H 4	100.0±5.8	100.0±5.8
4921.93	4923.76	He I	1.07±0.15	1.06±0.15
4958.91	4960.98	[O III]	299±17	296±18
5006.84	5008.87	[O III]	850±49	838±52
5411.52	5413.44	He II	1.14±0.16	1.09±0.17
5517.66	5515.71	[Cl III]	0.54±0.10	0.72±0.15
5537.60	5536.92	[Cl III]	0.62±0.12	0.82±0.17
5754.60	5753.06	[N II]	1.65±0.15	2.17±0.24
5875.66	5874.38	He I	9.26±0.51	12.09±0.90
6233.80	6232.72	He II	0.90±0.13	1.16±0.17
6300.34	6298.11	[O I]	5.91±0.35	7.56±0.43
6310.80	6311.24	He II	1.19±0.13	1.52±0.17
6312.10	*	[S III]	*	*
6363.78	6361.78	[O I]	1.92±0.16	2.45±0.20
6548.10	6546.50	[N II]	32.4±1.7	40.9±1.8
6562.77	6561.26	H 3	226.5±11.6	286.3±12.3
6583.50	6581.87	[N II]	94.6±4.9	119.2±5.1
6678.16	6676.58	He I	2.61±0.16	3.27±0.18
6716.44	6714.74	[S II]	18.01±0.93	22.60±1.02
6730.82	6729.11	[S II]	13.05±0.68	16.36±0.75
7065.25	7063.38	He I	1.53±0.14	1.88±0.18
7135.80	7133.55	[Ar III]	10.8±0.61	13.3±0.89

$c(\text{H}\beta) = 0.16 \pm 0.26$

$I_{\text{ob}}(\text{H}\beta) = 3.629 \times 10^{-13} \text{ erg cm}^{-2} \text{ s}^{-1}$

$I(\text{H}\beta) = 5.246 \times 10^{-13} \text{ erg cm}^{-2} \text{ s}^{-1}$

Extraction window = 2'' × 42''

NGC 6210

3679.36	3678.99	H 21	0.82±0.55	0.94±0.65
3682.81	*	H 20	*	*
3703.86	3703.35	H 16	3.19±0.20	3.68±0.50
3705.02	*	He I	*	*
3711.97	3710.81	H 15	1.26±0.11	1.45±0.22
3726.03	3726.58	[O II]	34.7±2.0	39.9±5.3
3728.82	*	[O II]	*	*
3734.37	3734.36	H 13	1.65±0.12	1.90±0.26
3750.15	3749.37	H 12	2.73±0.19	3.13±0.42
3756.10	3756.41	He I	1.17±0.11	1.35±0.20
3757.21	*	O III	*	*
3770.63	3770.16	H 11	3.84±0.25	4.41±0.58
3797.90	3797.04	H 10	4.26±0.26	4.88±0.63
3819.62	3818.55	He I	1.10±0.11	1.26±0.19
3835.39	3834.65	H 9	6.78±0.40	7.73±0.97
3856.02	3857.28	Si II	0.40±0.08	0.46±0.10
3856.13	*	O II	*	*
3868.75	3868.05	[Ne III]	75.9±4.3	86±10
3888.65	3888.18	H 8	17.8±1.0	20.2±2.4
3889.05	*	He I	*	*
3907.46	3908.76	O II	0.145±0.058	0.164±0.068
3918.98	3917.87	C II	0.252±0.072	0.285±0.087
3920.68	*	C II	*	*
3967.46	3967.66	[Ne III]	39.8±2.3	44.7±5.1
3970.07	*	H 7	*	*
4009.26	4008.78	He I	0.701±0.081	0.78±0.12
4026.21	4025.47	He I	2.47±0.16	2.75±0.31
4068.60	4068.56	[S II]	1.54±0.11	1.71±0.19
4069.89	*	O II	*	*

TABLE 2  
–continued

$\lambda(\text{\AA})$	$\lambda_{\text{ob}}(\text{\AA})$	Ion	$I_{\text{ob}}(\lambda)$	$I(\lambda)$
NGC 6210 (cont.)				
4072.16	4075.60	O II	0.681±0.076	0.76±0.11
4075.86	*	O II	*	*
4076.35	*	[S II]	*	*
4083.90	4083.58	O II	0.066±0.038	0.073±0.043
4085.11	*	O II	*	*
4087.15	4088.47	O II	0.194±0.048	0.215±0.056
4089.29	*	O II	*	*
4092.93	*	O II	*	*
4101.74	4101.01	H 6	25.1±1.4	27.8±2.8
4120.84	4119.33	He I	0.275±0.061	0.304±0.072
4143.76	4144.06	He I	0.529±0.063	0.582±0.084
4257.80	4259.57	Ne II	0.154±0.058	0.167±0.063
4267.15	4265.90	C II	0.610±0.071	0.659±0.089
4275.55	4275.35	O II	0.193±0.048	0.208±0.054
4276.75	*	O II	*	*
4283.73	4285.33	O II	0.110±0.026	0.118±0.030
4285.69	*	O II	*	*
4315.40	4316.52	O II	0.283±0.038	0.304±0.045
4315.83	*	O II	*	*
4317.14	*	O II	*	*
4340.47	4339.84	H 5	43.7±2.5	46.8±3.8
4363.21	4362.56	[O III]	5.95±0.34	6.35±0.50
4379.11	4377.94	N III	0.094±0.028	0.10±0.030
4379.55	*	Ne II	*	*
4387.93	4387.65	He I	0.646±0.050	0.688±0.064
4391.94	*	Ne II	*	*
4409.30	4407.75	Ne II	0.100±0.029	0.106±0.031
4413.11	4412.70	Ne II	0.077±0.029	0.081±0.031
4413.22	*	Ne II	*	*
4413.78	*	[Fe II]	*	*
4414.90	*	O II	*	*
4428.54	4427.57	Ne II	0.158±0.033	0.168±0.035
4430.94	*	Ne II	*	*
4457.05	4455.12	Ne II	0.076±0.033	0.080±0.035
4457.24	*	Ne II	*	*
4465.41	4464.00	O II	0.065±0.030	0.068±0.031
4471.50	4470.81	He I	5.22±0.30	5.49±0.39
4571.10	4571.64	Mg I]	0.188±0.038	0.195±0.040
4630.54	4634.30	N II	0.466±0.039	0.480±0.042
4634.14	*	N III	*	*
4638.86	4640.29	O II	1.104±0.072	1.135±0.078
4640.64	*	N III	*	*
4641.81	*	O II	*	*
4649.13	4648.54	O II	0.751±0.058	0.771±0.062
4650.84	*	O II	*	*
4658.10	4658.80	[Fe III]	0.397±0.045	0.407±0.047
4661.63	*	O II	*	*
4673.73	4673.26	O II	0.174±0.036	0.178±0.038
4676.21	*	O II	*	*
4685.68	4684.94	He II	2.27±0.14	2.32±0.14
4696.35	4695.34	O II	0.042±0.022	0.043±0.022
4699.22	*	O II	*	*
4701.59	*	[Fe III]	*	*
4711.37	4711.00	[Ar IV]	2.09±0.13	2.13±0.13
4713.17	*	He I	*	*
4740.17	4739.25	[Ar IV]	1.563±0.098	1.59±0.10
4777.88	4779.30	[Fe III]	0.065±0.027	0.066±0.028
4783.34	4786.29	O IV	0.073±0.029	0.074±0.030
4785.90	*	C IV	*	*
4788.13	*	N II	*	*
4861.33	4860.16	H 4	100.0±5.7	100.0±5.7
4881.11	4883.96	[Fe III]	0.0316±0.024	0.032±0.024
4921.93	4920.77	He I	1.492±0.093	1.482±0.093
4924.53	*	O II	*	*
4931.80	4931.37	[O III]	0.558±0.049	0.554±0.049
4958.91	4957.53	[O III]	346±20	342±20
5006.84	5005.38	[O III]	985±56	968±57
5047.74	5046.44	He I	0.154±0.015	0.151±0.015
5191.82	5189.29	[Ar III]	0.054±0.012	0.053±0.012
5197.90	5197.10	[N I]	0.127±0.014	0.123±0.014
5200.26	*	[N I]	*	*
5342.38	5341.23	C II	0.016±0.010	0.0157±0.0099
5411.52	5410.37	He II	0.135±0.015	0.127±0.016

TABLE 2  
–continued

$\lambda(\text{\AA})$	$\lambda_{\text{ob}}(\text{\AA})$	Ion	$I_{\text{ob}}(\lambda)$	$I(\lambda)$
NGC 6210 (cont.)				
5517.66	5515.53	[Cl III]	0.346±0.024	0.325±0.029
5537.60	5535.62	[Cl III]	0.415±0.028	0.389±0.034
5754.60	5753.91	[N II]	0.527±0.035	0.457±0.034
5801.51	5800.08	C IV	0.111±0.019	0.096±0.017
5812.14	5810.49	C IV	0.110±0.019	0.095±0.017
5875.66	5874.48	He I	18.20±0.91	15.67±0.86
5931.78	5931.30	N II	0.0581±0.0097	0.0498±0.0084
5941.65	5942.91	N II	0.036±0.011	0.0308±0.0091
6036.70	6036.99	He II	0.0010±0.0085	0.0087±0.0072
6101.83	6100.16	[K IV]	0.101±0.013	0.086±0.011
6157.42	6158.36	Ni II	0.0214±0.0093	0.0181±0.0078
6157.60	*	[Mn V]	*	*
6300.30	6299.32	[O I]	2.66±0.14	2.23±0.10
6312.10	6310.85	[S III]	1.322±0.069	1.108±0.052
6310.80	*	He II	*	*
6363.78	6362.80	[O I]	0.888±0.048	0.742±0.036
6461.95	6460.37	C II	0.081±0.014	0.067±0.012
6548.10	6546.89	[N II]	8.75±0.44	7.24±0.31
6562.77	6561.29	H 3	345±17	284.9±12.1
6583.50	6582.05	[N II]	23.7±1.2	19.57±0.83
6678.16	6676.48	He I	5.18±0.26	4.25±0.19
6716.44	6714.88	[S II]	2.80±0.15	2.30±0.11
6730.82	6729.20	[S II]	4.64±0.24	3.80±0.17
7065.25	7062.96	He I	6.19±0.31	4.97±0.25
7135.80	7133.30	[Ar III]	13.01±0.65	10.40±0.53
7281.35	7279.45	He I	0.63±0.04	0.498±0.032
7319.99	7316.92	[O II]	2.82±0.15	2.23±0.13
7329.67	7327.67	[O II]	2.38±0.12	1.88±0.11

c(H $\beta$ ) = 0.19 ± 0.16 $I_{\text{o}}$  (H $\beta$ ) = 2.083 × 10<sup>-14</sup> erg cm<sup>-2</sup> s<sup>-1</sup> $I$ (H $\beta$ ) = 3.226 × 10<sup>-13</sup> erg cm<sup>-2</sup> s<sup>-1</sup>

Extraction window = 2'' × 16''

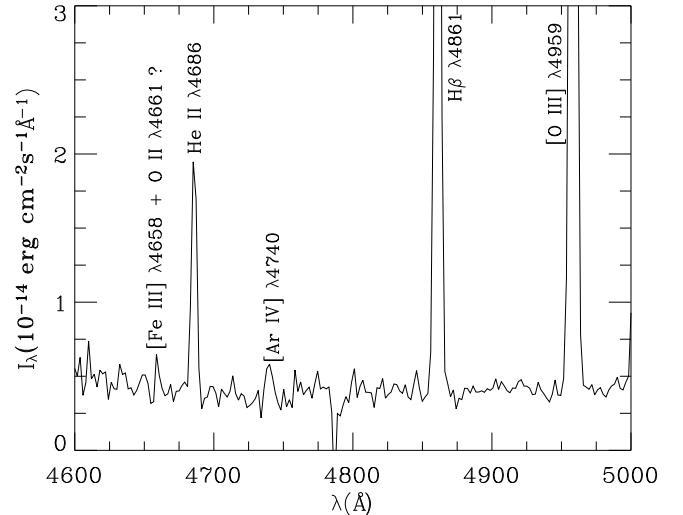


FIG. 2.— Part of the blue spectra of JnEr 1 showing the feature used to derive upper limits to the Fe abundance.

(see more details in Section 5). The physical conditions and the O<sup>+</sup>/H<sup>+</sup> and O<sup>++</sup>/H<sup>+</sup> abundance ratios were calculated with the IRAF NEBULAR package. However, we changed the atomic data for [Cl III] and used the transition probabilities of Mendoza & Zeippen (1982) and the collision strengths of Mendoza (1983), because these data lead to densities that are in bet-

TABLE 3  
 PHYSICAL CONDITIONS

Object	PNG <sup>a</sup>	$T_e(\text{[N II]})$ (K)	$T_e(\text{[O III]})$ (K)	$n_e(\text{[S II]})$ ( $\text{cm}^{-3}$ )	$n_e(\text{[Cl III]})$ ( $\text{cm}^{-3}$ )	$n_e(\text{[Ar IV]})$ ( $\text{cm}^{-3}$ )	$n_e$ (adopted) ( $\text{cm}^{-3}$ )	Ref.
Cn 3-1	038.2+12.0	7600 ± 300	7700 <sup>+500</sup> <sub>-300</sub>	9400 <sup>+12300</sup> <sub>-3600</sub>	12200 <sup>+3200</sup> <sub>-2300</sub>	...	11900 ± 1600	1
Hu 1-1	119.6-06.7	11500 ± 400	12100 ± 300	1500 <sup>+1400</sup> <sub>-300</sub>	< 100	2600 <sup>+1100</sup> <sub>-900</sub>	1600 ± 300	1
IC 418	215.2-24.2	9100 <sup>+600</sup> <sub>-500</sub>	8800 ± 200	29200 <sup>+19100</sup> <sub>-19100</sub>	13400 <sup>+3000</sup> <sub>-2200</sub>	7000 <sup>+8200</sup> <sub>-3900</sub>	12400 ± 2400	2
IC 1747	130.2+01.3	12300 <sup>+700</sup> <sub>-600</sub>	10700 <sup>+300</sup> <sub>-200</sub>	5000 <sup>+2300</sup> <sub>-1300</sub>	...	3600 <sup>+1100</sup> <sub>-900</sub>	3900 ± 900	1
IC 3568	123.6+34.5	18800 <sup>+4500</sup> <sub>-2600</sub>	11400 ± 300	2000 <sup>+1500</sup> <sub>-800</sub>	...	2500 <sup>+1000</sup> <sub>-900</sub>	2300 ± 700	3
IC 4191	304.5-04.8	11100 <sup>+600</sup> <sub>-500</sub>	9900 ± 200	8300 <sup>+6400</sup> <sub>-2700</sub>	13600 <sup>+2400</sup> <sub>-1900</sub>	17200 <sup>+2900</sup> <sub>-2300</sub>	14900 ± 1400	4
IC 4406	319.6+15.7	10300 ± 300	10000 ± 200	1000 <sup>+200</sup> <sub>-200</sub>	4500 <sup>+900</sup> <sub>-800</sub>	1500 <sup>+900</sup> <sub>-700</sub>	1300 ± 200	4
IC 4593	025.3+40.8	9700 <sup>+1300</sup> <sub>-900</sub>	8500 <sup>+300</sup> <sub>-200</sub>	2000 <sup>+700</sup> <sub>-500</sub>	800 <sup>+1600</sup> <sub>-1600</sub>	...	1900±500	5
IC 4846	027.6-09.6	11900 <sup>+3100</sup> <sub>-700</sub>	10500 <sup>+500</sup> <sub>-400</sub>	6900 <sup>+18900</sup> <sub>-3200</sub>	12600 <sup>+63100</sup> <sub>-7400</sub>	10700 <sup>+4400</sup> <sub>-3000</sub>	10400 ± 3300	6
IC 5217	100.6-05.4	13600 <sup>+6000</sup> <sub>-2500</sub>	10700 <sup>+500</sup> <sub>-400</sub>	4800 <sup>+3900</sup> <sub>-1700</sub>	4300 <sup>+3500</sup> <sub>-2000</sub>	6400 <sup>+4500</sup> <sub>-2800</sub>	5000 ± 1700	7
JnEr 1	164.8+31.1	10300 <sup>+1000</sup> <sub>-800</sub>	11700 <sup>+800</sup> <sub>-600</sub>	200 <sup>+500</sup> <sub>-600</sub>	...	...	200 <sup>+500</sup> <sub>-180</sub>	5
M 1-73	051.9-03.8	8500 <sup>+1300</sup> <sub>-600</sub>	7200 ± 100	5900 <sup>+3800</sup> <sub>-1800</sub>	...	...	5900 ± 2800	1
MyCn 18	307.5-04.9	9700 <sup>+500</sup> <sub>-400</sub>	7300 ± 100	5500 <sup>+3000</sup> <sub>-1500</sub>	12800 <sup>+2300</sup> <sub>-1800</sub>	...	9500 ± 1500	4
NGC 40	120.0+09.8	8600 <sup>+300</sup> <sub>-200</sub>	10600 <sup>+300</sup> <sub>-200</sub>	1800 <sup>+600</sup> <sub>-400</sub>	1100 <sup>+500</sup> <sub>-400</sub>	...	1400 ± 300	3
NGC 2392	197.8+17.3	12700 <sup>+2200</sup> <sub>-1400</sub>	14500 <sup>+1100</sup> <sub>-900</sub>	2600 <sup>+22000</sup> <sub>-1600</sub>	2100 <sup>+2000</sup> <sub>-1300</sub>	1200 <sup>+1800</sup> <sub>-1300</sub>	1700 ± 1200	5
NGC 3132	272.1+12.3	9700 <sup>+300</sup> <sub>-200</sub>	9500 ± 200	600 <sup>+200</sup> <sub>-100</sub>	800 <sup>+500</sup> <sub>-400</sub>	700 <sup>+800</sup> <sub>-700</sub>	600 ± 100	4
NGC 3242	261.0+32.0	12100 <sup>+1700</sup> <sub>-1100</sub>	11800 ± 300	2300 <sup>+500</sup> <sub>-500</sub>	1300 <sup>+900</sup> <sub>-500</sub>	3300 <sup>+1100</sup> <sub>-900</sub>	2000 ± 400	4
NGC 3587	148.4+57.0	9800 <sup>+900</sup> <sub>-700</sub>	11600 ± 500	< 100	...	...	100 <sup>+400</sup> <sub>-80</sub>	5
NGC 5882	327.8+10.0	10500 <sup>+500</sup> <sub>-400</sub>	9400 ± 200	4900 <sup>+2400</sup> <sub>-1300</sub>	4400 <sup>+1000</sup> <sub>-800</sub>	6400 <sup>+1400</sup> <sub>-1200</sub>	5000 ± 700	4
NGC 6153	341.8+05.4	10300 ± 400	9100 ± 200	4200 <sup>+1800</sup> <sub>-1100</sub>	5000 <sup>+1000</sup> <sub>-900</sub>	3000 <sup>+1000</sup> <sub>-800</sub>	4000 ± 600	8
NGC 6210	043.1+37.7	11600 <sup>+700</sup> <sub>-600</sub>	10000±300	4300 <sup>+1600</sup> <sub>-1000</sub>	4400 <sup>+1800</sup> <sub>-1300</sub>	7200 <sup>+2900</sup> <sub>-2100</sub>	4700±900	5
NGC 6210	043.1+37.7	11100 <sup>+500</sup> <sub>-400</sub>	9600±200	4200 <sup>+1800</sup> <sub>-1100</sub>	4100 <sup>+900</sup> <sub>-800</sub>	9000 <sup>+1400</sup> <sub>-1400</sub>	5000±700	3
NGC 6543	096.4+29.9	10000 ± 400	7900 ± 100	6900 <sup>+4900</sup> <sub>-2200</sub>	6400 <sup>+1200</sup> <sub>-1000</sub>	4400 <sup>+1100</sup> <sub>-900</sub>	5400 ± 700	9
NGC 6572	034.6+11.8	11200 <sup>+800</sup> <sub>-600</sub>	10300 <sup>+300</sup> <sub>-200</sub>	25200 <sup>+13600</sup> <sub>-13600</sub>	20000 <sup>+3800</sup> <sub>-2900</sub>	23200 <sup>+3800</sup> <sub>-3100</sub>	21600 ± 2400	3
NGC 6720	063.1+13.9	10600 ± 300	10600 <sup>+300</sup> <sub>-200</sub>	500 <sup>+200</sup> <sub>-100</sub>	500 <sup>+500</sup> <sub>-400</sub>	1400 <sup>+900</sup> <sub>-700</sub>	500 ± 100	3
NGC 6803	046.4-04.1	10200 <sup>+500</sup> <sub>-400</sub>	9600 ± 200	8300 <sup>+6800</sup> <sub>-2700</sub>	11600 <sup>+2100</sup> <sub>-1700</sub>	12900 <sup>+2200</sup> <sub>-1800</sub>	11900 ± 1300	1
NGC 6826	083.5+12.7	10600 <sup>+600</sup> <sub>-500</sub>	9300 ± 200	1900 <sup>+600</sup> <sub>-400</sub>	1600 <sup>+900</sup> <sub>-500</sub>	3100 <sup>+1000</sup> <sub>-900</sub>	1900 ± 300	3
NGC 6884	082.1+07.0	11500 <sup>+600</sup> <sub>-500</sub>	11000 ± 300	8200 <sup>+6400</sup> <sub>-2600</sub>	6900 <sup>+1300</sup> <sub>-1100</sub>	14500 <sup>+2500</sup> <sub>-2000</sub>	8600 ± 1000	3
NGC 7026	089.0+00.3	9300 ± 400	9200 ± 200	...	15600 <sup>+4300</sup> <sub>-3000</sub>	7700 <sup>+1500</sup> <sub>-1300</sub>	9100 ± 1100	1

REFERENCES. — *Line intensities from:* (1) Wesson et al. (2005), (2) Sharpee et al. (2003), (3) Liu et al. (2004b), (4) Tsamis et al. (2003), (5) this work, (6) Hyung et al. (2001b), (7) Hyung et al. (2001a), (8) Liu et al. (2000), (9) Wesson & Liu (2004).

<sup>a</sup> PNG identifications from Acker et al. (1992).

ter agreement with the values implied by the other diagnostics. To derive the  $\text{He}^+$  abundance we used the calculations of Benjamin et al. (1999) and the He I  $\lambda 6678$  line, since it is the brightest of the measured singlet lines and singlet lines are not affected by self-absorption effects. The  $\text{He}^{++}$  abundance was calculated using the He II  $\lambda 4686$  line and the emissivities of Storey & Hummer (1995). We also used the emissivities of Storey & Hummer (1995) for H I. The errors in the  $\text{O}^+$  and  $\text{O}^{++}$  abundances have been derived by adding quadratically the errors in the line intensity ratio used and the errors arising from the uncertainties in  $T_e$  and  $n_e$ . Columns 2, 3, 4, and 5 in Table 4 show our derived ionic abundances for  $\text{He}^+$ ,  $\text{He}^{++}$ ,  $\text{O}^+$ , and  $\text{O}^{++}$ .

#### 4.1. [Fe III] lines and $\text{Fe}^{++}$ abundances

To derive the  $\text{Fe}^{++}$  abundance we solved the equations of statistical equilibrium (see, e.g., Osterbrock & Ferland 2006) for the lowest 34 levels and used the collision strengths of Zhang (1996) and the transition probabilities of Quinet (1996). We calculated the  $\text{Fe}^{++}$  abundance using up to 10 [Fe III] lines among the follow-

ing:  $\lambda 4080$ ,  $\lambda 4607$ ,  $\lambda 4667$ ,  $\lambda 4658$ ,  $\lambda 4701$ ,  $\lambda 4734$ ,  $\lambda 4755$ ,  $\lambda 4769$ ,  $\lambda 4778$ ,  $\lambda 4881$ ,  $\lambda 4986$ ,  $\lambda 5412$ , and  $\lambda 5270$ . When several lines were measured, we rejected those that led to  $\text{Fe}^{++}$  abundances much larger than the rest, since this could be due to contamination of these [Fe III] lines with other weak lines. The final  $\text{Fe}^{++}$  abundance is the weighted mean of all the abundances derived with the available lines (with weights  $1/\sigma^2$  where  $\sigma$  comes from the errors in the line intensities). The spectra we used from the literature have a resolution better than 2 Å in the blue range, but our observed spectra have a resolution of about 4 Å and [Fe III]  $\lambda 4658$  is blended with O II  $\lambda 4661$ . In order to deblend these lines we used a multiple Gaussian profile-fitting procedure in IC 4593, and this procedure worked properly in this object since the  $\text{Fe}^{++}$  abundance we obtain from this [Fe III] line is in good agreement with the results obtained with the other four [Fe III] lines measured in this PN. However, the multiple Gaussian fit did not work in NGC 6210 and NGC 2392. For NGC 6210, we corrected for the contribution of O II  $\lambda 4661$  using the intensity we measured for O II  $\lambda\lambda 4672$ , 4676 lines and the expected relative inten-



TABLE 4  
 IONIC AND TOTAL ABUNDANCES:  $\{X^{+i}\} = 12 + \log(X^{+i}/H^+)$ ,  $\{X\} = 12 + \log(X/H)$

Object <sup>a</sup> (1)	{He <sup>+</sup> } (2)	{He <sup>++</sup> } (3)	{O <sup>+</sup> } (4)	{O <sup>++</sup> } (5)	ICF (6)	{O} (7)	{Fe <sup>+</sup> } (8)	{Fe <sup>++</sup> } (9)	N <sup>b</sup> (10)	{Fe} <sup>c</sup> (11)	{Fe} <sup>d</sup> (12)
Cn3-1	10.67	7.52	8.80 ± 0.11	7.27 <sup>+0.08</sup> <sub>-0.10</sub>	1.00	8.81 ± 0.11	–	5.62 <sup>+0.04</sup> <sub>-0.05</sub>	3	5.71 <sup>+0.14</sup> <sub>-0.16</sub>	5.63 <sup>+0.15</sup> <sub>-0.17</sub>
Hu 1-1	10.93	10.18	7.99 ± 0.06	8.38 <sup>+0.03</sup> <sub>-0.04</sub>	1.11	8.57 ± 0.03	–	4.25 <sup>+0.16</sup> <sub>-0.25</sub>	1	4.76 <sup>+0.17</sup> <sub>-0.27</sub>	4.65 <sup>+0.17</sup> <sub>-0.27</sub>
IC 418	10.97	–	8.47 <sup>+0.13</sup> <sub>-0.15</sub>	8.08 ± 0.03	1.00	8.62 ± 0.10	3.93:	4.14 <sup>+0.06</sup> <sub>-0.08</sub>	10	4.27 <sup>+0.16</sup> <sub>-0.20</sub>	4.50 <sup>+0.16</sup> <sub>-0.20</sub>
IC 1747	11.01	10.04	7.09 <sup>+0.10</sup> <sub>-0.09</sub>	8.54 ± 0.03	1.07	8.58 ± 0.03	–	< 4.34	–	< 5.67	< 5.04
IC 3568	10.96	9.02	5.72 <sup>+0.18</sup> <sub>-0.10</sub>	8.37 ± 0.04	1.01	8.37 ± 0.04	–	3.82 <sup>+0.12</sup> <sub>-0.16</sub>	2	6.21 <sup>+0.20</sup> <sub>-0.20</sub>	4.98 <sup>+0.16</sup> <sub>-0.22</sub>
IC 4191	11.05	10.08	7.56 <sup>+0.09</sup> <sub>-0.10</sub>	8.70 ± 0.03	1.07	8.76 ± 0.03	–	4.42 <sup>+0.10</sup> <sub>-0.12</sub>	1	5.48 <sup>+0.12</sup> <sub>-0.16</sub>	5.00 <sup>+0.11</sup> <sub>-0.15</sub>
IC 4406	10.97	10.08	8.24 ± 0.06	8.57 ± 0.03	1.08	8.77 ± 0.03	–	< 4.55	–	< 5.02	< 4.94
IC 4593	11.01	8.54	7.45 <sup>+0.20</sup> <sub>-0.24</sub>	8.55 ± 0.04	1.00	8.58 ± 0.04	–	5.36 <sup>+0.09</sup> <sub>-0.11</sub>	4	6.36 <sup>+0.20</sup> <sub>-0.27</sub>	5.90 <sup>+0.14</sup> <sub>-0.18</sub>
IC 4846	10.97	8.69	7.07 <sup>+0.14</sup> <sub>-0.39</sub>	8.50 <sup>+0.04</sup> <sub>-0.05</sub>	1.00	8.51 <sup>+0.04</sup> <sub>-0.05</sub>	–	4.55 <sup>+0.10</sup> <sub>-0.13</sub>	3	5.83 <sup>+0.16</sup> <sub>-0.41</sub>	5.20 <sup>+0.14</sup> <sub>-0.23</sub>
IC 5217	10.84	9.96	6.60 <sup>+0.33</sup> <sub>-0.47</sub>	8.63 <sup>+0.04</sup> <sub>-0.05</sub>	1.08	8.67 <sup>+0.04</sup> <sub>-0.05</sub>	–	4.62 <sup>+0.26</sup> <sub>-0.45</sub>	1	6.49 <sup>+0.37</sup> <sub>-0.98</sub>	5.56 <sup>+0.30</sup> <sub>-0.58</sub>
JnEr 1	11.32	10.24	8.42 <sup>+0.16</sup> <sub>-0.17</sub>	7.98 <sup>+0.05</sup> <sub>-0.06</sub>	1.06	8.58 ± 0.12	–	< 6.00	–	< 6.15	< 6.16
M 1-73	11.03	9.00	8.27 <sup>+0.16</sup> <sub>-0.20</sub>	8.54 <sup>+0.06</sup> <sub>-0.04</sub>	1.01	8.73 ± 0.06	–	5.45 <sup>+0.08</sup> <sub>-0.10</sub>	2	5.85 <sup>+0.17</sup> <sub>-0.24</sub>	5.80 <sup>+0.13</sup> <sub>-0.16</sub>
MyCn 18	10.95	8.66	7.83 <sup>+0.09</sup> <sub>-0.11</sub>	8.52 ± 0.02	1.00	8.60 ± 0.03	–	5.47 ± 0.03	6	6.14 <sup>+0.09</sup> <sub>-0.11</sub>	5.88 <sup>+0.07</sup> <sub>-0.08</sub>
NGC 40	10.80	7.56	8.63 <sup>+0.06</sup> <sub>-0.08</sub>	7.07 <sup>+0.03</sup> <sub>-0.05</sub>	1.00	8.64 <sup>+0.06</sup> <sub>-0.08</sub>	4.86:	5.58 ± 0.02	7	5.67 <sup>+0.08</sup> <sub>-0.11</sub>	5.67 <sup>+0.08</sup> <sub>-0.12</sub>
NGC 2392	10.90	10.46	7.41 <sup>+0.19</sup> <sub>-0.26</sub>	8.07 <sup>+0.05</sup> <sub>-0.06</sub>	1.23	8.25±0.06	–	5.62 <sup>+0.07</sup> <sub>-0.08</sub>	5	6.35 <sup>+0.19</sup> <sub>-0.27</sub>	6.11 <sup>+0.14</sup> <sub>-0.19</sub>
NGC 3132	11.04	9.51	8.42 <sup>+0.05</sup> <sub>-0.06</sub>	8.52 ± 0.03	1.02	8.78 ± 0.03	–	4.99 <sup>+0.03</sup> <sub>-0.04</sub>	6	5.30 <sup>+0.06</sup> <sub>-0.08</sub>	5.35 <sup>+0.06</sup> <sub>-0.08</sub>
NGC 3242	10.90	10.34	6.53 <sup>+0.16</sup> <sub>-0.20</sub>	8.41 ± 0.03	1.18	8.49 ± 0.03	–	3.84 <sup>+0.12</sup> <sub>-0.17</sub>	2	5.60 <sup>+0.18</sup> <sub>-0.28</sub>	4.75 <sup>+0.15</sup> <sub>-0.21</sub>
NGC 3587	10.94	10.15	8.09 <sup>+0.15</sup> <sub>-0.16</sub>	8.27 <sup>+0.04</sup> <sub>-0.05</sub>	1.11	8.53 ± 0.07	–	5.24 <sup>+0.36</sup> <sub>-0.27</sub>	1	5.62 <sup>+0.37</sup> <sub>-0.36</sub>	5.62 <sup>+0.37</sup> <sub>-0.32</sub>
NGC 5882	11.02	9.35	6.92 <sup>+0.08</sup> <sub>-0.09</sub>	8.66 ± 0.03	1.01	8.67 ± 0.03	–	4.73 <sup>+0.04</sup> <sub>-0.05</sub>	6	6.30 <sup>+0.09</sup> <sub>-0.11</sub>	5.52 <sup>+0.08</sup> <sub>-0.09</sub>
NGC 6153	11.06	10.05	7.20 <sup>+0.08</sup> <sub>-0.08</sub>	8.62 ± 0.03	1.06	8.67 ± 0.03	–	4.50 <sup>+0.06</sup> <sub>-0.08</sub>	3	5.80 <sup>+0.10</sup> <sub>-0.12</sub>	5.18 <sup>+0.09</sup> <sub>-0.11</sub>
NGC 6210 <sup>e</sup>	10.99	9.09	7.16 <sup>+0.10</sup> <sub>-0.11</sub>	8.54 <sup>+0.03</sup> <sub>-0.04</sub>	1.01	8.56±0.03	–	4.62 <sup>+0.08</sup> <sub>-0.10</sub>	2	5.87 <sup>+0.12</sup> <sub>-0.15</sub>	5.26 <sup>+0.11</sup> <sub>-0.14</sub>
NGC 6210 <sup>f</sup>	11.01	9.28	7.21 <sup>+0.17</sup> <sub>-0.08</sub>	8.62±0.04	1.01	8.64±0.04	–	4.60 <sup>+0.04</sup> <sub>-0.05</sub>	8	5.88 <sup>+0.08</sup> <sub>-0.10</sub>	5.26 <sup>+0.09</sup> <sub>-0.11</sub>
NGC 6543	11.05	–	7.24 ± 0.08	8.75 ± 0.03	1.00	8.76±0.03	–	4.90 ± 0.04	7	6.26 <sup>+0.09</sup> <sub>-0.10</sub>	5.59 <sup>+0.08</sup> <sub>-0.09</sub>
NGC 6572	11.01	8.53	7.59 <sup>+0.10</sup> <sub>-0.13</sub>	8.58 ± 0.04	1.00	8.62 <sup>+0.03</sup> <sub>-0.04</sub>	–	4.55 ± 0.06	7	5.46 <sup>+0.11</sup> <sub>-0.15</sub>	5.05 <sup>+0.09</sup> <sub>-0.13</sub>
NGC 6720	10.97	10.25	8.21 ± 0.06	8.47 <sup>+0.03</sup> <sub>-0.05</sub>	1.12	8.71 <sup>+0.03</sup> <sub>-0.04</sub>	4.28:	4.70 <sup>+0.04</sup> <sub>-0.05</sub>	4	5.14 <sup>+0.07</sup> <sub>-0.08</sub>	5.09 <sup>+0.07</sup> <sub>-0.09</sub>
NGC 6803	11.04	9.56	7.51 <sup>+0.08</sup> <sub>-0.10</sub>	8.64 ± 0.04	1.02	8.68 ± 0.04	–	4.90 ± 0.04	3	5.93 <sup>+0.09</sup> <sub>-0.10</sub>	5.45 <sup>+0.08</sup> <sub>-0.10</sub>
NGC 6826	11.00	7.34	6.99 <sup>+0.09</sup> <sub>-0.11</sub>	8.52 ± 0.04	1.00	8.53 ± 0.04	–	4.72 ± 0.05	5	6.10 <sup>+0.10</sup> <sub>-0.12</sub>	5.42 <sup>+0.10</sup> <sub>-0.12</sub>
NGC 6884	10.87	10.19	7.16 <sup>+0.08</sup> <sub>-0.09</sub>	8.55 ± 0.04	1.13	8.62 ± 0.04	4.04:	4.74 ± 0.04	6	6.04 <sup>+0.09</sup> <sub>-0.11</sub>	5.44 <sup>+0.10</sup> <sub>-0.11</sub>
NGC 7026	11.04	10.12	7.86±0.10	8.62 ± 0.04	1.08	8.72 ± 0.04	–	< 4.73	–	< 5.49	< 5.19

<sup>a</sup> Line intensities from the same references of Table 3.

<sup>b</sup> Number of [Fe III] lines used in the Fe<sup>++</sup> abundance determination.

<sup>c</sup> Derived using equation (1).

<sup>d</sup> Derived using equations (2) and (3).

<sup>e</sup> Line intensities from our observations.

<sup>f</sup> Line intensities from Liu et al. (2004b).

sities of the O II recombination lines from the same multiplet (Peimbert & Peimbert 2005). We did not measure any O II recombination line in NGC 2392, but the contribution of O II  $\lambda 4661$  to the [Fe III]  $\lambda 4658$  line should not be important in this object, since the Fe<sup>++</sup> abundance derived from [Fe III]  $\lambda 4658$  is consistent with the abundances obtained from the other five [Fe III] lines. In NGC 3587 we only measured the line [Fe III]  $\lambda 4986$  (see Figure 1), which is the brightest line for the physical conditions of this nebula.

Three of the PNe from the literature have no identifications of [Fe III] lines in their spectra and we used recombination lines measured near 4658 Å (since [Fe III]  $\lambda 4658$  should be the brightest line for the physical conditions of these objects) to derive upper limits to the Fe<sup>++</sup> abundance. The lines used are C IV  $\lambda 4659$  for IC 1747 and NGC 7026, and O II  $\lambda 4661$  for IC 4406. We also calculated upper limits to the Fe<sup>++</sup> abundance for JnEr 1, where the detection of [Fe III] lines is uncertain (see Figure 2).

Column 9 in Table 4 shows the Fe<sup>++</sup> abundance we

obtained for each PN, and Column 10 shows the number of [Fe III] lines that were used for each PN to calculate the final Fe<sup>++</sup> abundance. The error in the Fe<sup>++</sup> abundance derived from each line was calculated in the same way described above for O<sup>+</sup> and O<sup>++</sup>, and when several lines of [Fe III] were measured we calculated the weighted mean of the Fe<sup>++</sup> abundances and used propagation of errors. Two entries for NGC 6210 are given in Tables 3 and 4. The first one shows the results obtained using our observations of this object; the second entry shows the results we derived using the spectrum measured by Liu et al. (2004b). The results implied by the two spectra are very similar.

#### 4.2. Other ionization states of Fe

As we mentioned in Section 1, the abundance of Fe<sup>+</sup> is often negligible, even for low-ionization objects. Four of the sample PNe have measurements of [Fe II] lines: IC 418, NGC 40, NGC 6720, and NGC 6884. Since [Fe II]  $\lambda 8616$  is almost insensitive to fluorescence effects (Lucy 1995), we used this line to calculate the Fe<sup>+</sup> abundance

in IC 418. The other three PNe had no measurements of this line and we used the intensity of [Fe II]  $\lambda 7155$  and assumed the relation  $I([\text{Fe II}] \lambda 7155)/I([\text{Fe II}] \lambda 8616) \sim 1$  found by Rodríguez (1996) for H II regions, to get an estimate of the  $\text{Fe}^+$  abundance using the emissivities derived by Bautista & Pradhan (1996). Column 8 in Table 4 shows the results. All the  $\text{Fe}^+/\text{H}^+$  abundances we obtained are lower than the values of  $\text{Fe}^{++}/\text{H}^+$ , with  $\text{Fe}^+/\text{Fe}^{++} = 0.21, 0.46, 0.38,$  and  $0.18$  for NGC 40, IC 418, NGC 6720, and NGC 6884, respectively. Although the values of  $\text{Fe}^+$  are uncertain (see Rodríguez 2002), we have used them to derive Fe abundances with Equation (3). The effect of  $\text{Fe}^+$  on the total Fe abundance is relevant only for IC 418 and NGC 40, where Fe/H increases by 0.16 dex and 0.08 dex, respectively, after including this ion. We expect that for the rest of the PNe in the sample the contribution of  $\text{Fe}^+$  will be even less important.

Four PNe of the sample have measurements of lines from ions of higher ionization states than  $\text{Fe}^{+3}$ : [Fe V] lines in IC 3568, NGC 6153, NGC 6210, NGC 6720, NGC 6826, and NGC 6884; [Fe VI] lines in NGC 6884; and [Fe VII] lines in IC 5217, NGC 3132, NGC 6210, and NGC 6884. Since no atomic data are available to calculate the  $\text{Fe}^{+4}$  abundance from optical lines, we only calculated the ionic abundances of  $\text{Fe}^{+5}$  and  $\text{Fe}^{+6}$ . For  $\text{Fe}^{+5}$ , we solved the equations of statistical equilibrium for 19 levels, using the transition probabilities and collision strengths of Chen & Pradhan (1999, 2000). For the  $\text{Fe}^{+6}$  calculations, we used a model atom with 9 levels and the transition probabilities and collision strengths of Witthoef & Badnell (2008). The level energies in both cases are from the compilation of Sugar & Corliss (1985) listed by NIST<sup>2</sup>, and the physical conditions used are the values of  $T_e[\text{O III}]$  and  $n_e$  shown in Table 3.

The identification of [Fe VII]  $\lambda 6601$  in IC 5217 (Hyung et al. 2001a) is probably incorrect since this line leads to an unrealistic high abundance,  $\text{Fe}^{+6}/\text{H}^+ = 8 \times 10^{-4}$ , and besides, other lines of the same ion such as  $\lambda 4990, \lambda 5160, \lambda 5278,$  and  $\lambda 5720$ , which should be brighter by more than a factor of 30 for the physical conditions of this PN, are not present in the spectra. In the other objects, we find  $\text{Fe}^{+5}/\text{H}^+ = 6.0 \times 10^{-8}$  and  $\text{Fe}^{+6}/\text{H}^+ = 4.7 \times 10^{-8}$  for NGC 6884,  $\text{Fe}^{+6}/\text{H}^+ = 8.0 \times 10^{-8}$  for NGC 3132, and  $\text{Fe}^{+6}/\text{H}^+ = 1.23 \times 10^{-7}$  for NGC 6210. If we had used the emissivities of Nussbaumer & Storey (1978) for  $\text{Fe}^{+5}$ , the derived abundances would be higher by factors up to 1.7. In the case of  $\text{Fe}^{+6}$ , the transition probabilities of Keenan & Norrington (1987) and the collision strengths of Nussbaumer et al. (1982) would lead to abundances higher by factors up to 1.8.

These  $\text{Fe}^{+5}$  and  $\text{Fe}^{+6}$  abundances are high, with values similar to the derived  $\text{Fe}^{++}$  abundances, but we should consider them with caution. On the one hand, only one [Fe VII] line has been measured for these PNe, but we estimate that other [Fe VII] lines, such as  $\lambda 4893, \lambda 5722, \lambda 4990,$  or  $\lambda 6089$ , should be brighter by factors between 3 and 18 for the physical conditions of these objects. Besides, NGC 3132 and NGC 6210 can be considered

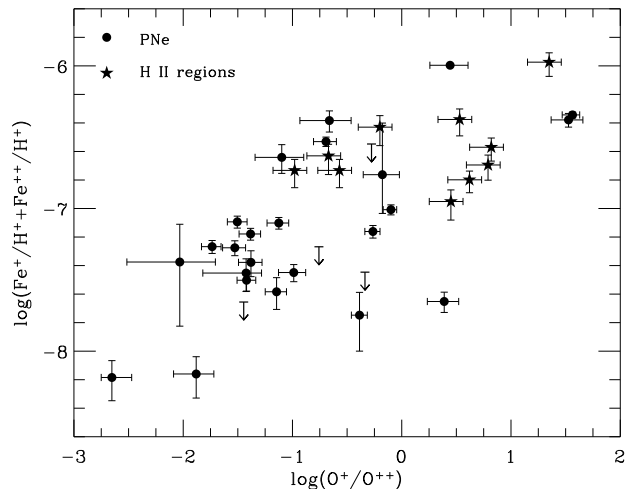


FIG. 3.— Values of  $\text{Fe}^+/\text{H}^+ + \text{Fe}^{++}/\text{H}^+$  as a function of the degree of ionization.

low-ionization PNe, since they have  $\text{He}^{++}/\text{H}^+ = 0.029$  and  $0.018$ , respectively, and hence we do not expect that high states of ionization contribute much to the total abundance of Fe in these objects. In fact, NGC 3132 does not have any [Fe V] or [Fe VI] line, and NGC 6210 only has [Fe V]  $\lambda 4227$ . On the other hand, some [Fe VI] lines can be affected by fluorescence effects (Chen & Pradhan 2000), and hence the real  $\text{Fe}^{+5}$  abundance for NGC 6884 could be lower than the one we calculated.

Nevertheless, we calculated what value of the total abundance of Fe we would get by adding all the calculated ionic abundances in these three PNe. We used the abundances derived for  $\text{Fe}^+, \text{Fe}^{++}, \text{Fe}^{+5},$  and  $\text{Fe}^{+6}$  and assumed that the ions we do not observe have abundances intermediate between those derived for the observed adjacent ions. The results we obtain in this way are intermediate between the Fe abundances derived in Section 5 using Equations (1) and (2)/(3) except for NGC 3132, where the Fe abundance calculated in this way ( $12 + \text{Fe}/\text{H} \sim 5.61$ ) is higher by a factor around 2. The agreement found for the other two objects may not be significant for the reasons mentioned above.

#### 4.3. Comparison with H II regions

For comparison purposes, we have selected from the literature a group of 10 Galactic H II regions (see Table 5) that have all the lines needed to carry out the same analysis we have performed for the PNe. We used the values of the ionic abundances of  $\text{Fe}^+, \text{Fe}^{++}, \text{O}^+,$  and  $\text{O}^{++}$  derived in the original papers since they were calculated using a similar procedure to the one we use for our sample PNe. Figure 3 shows the values of  $\text{Fe}^+/\text{H}^+ + \text{Fe}^{++}/\text{H}^+$  as a function of the degree of ionization (measured by the ratio  $\text{O}^+/\text{O}^{++}$ ) for all our sample objects. The objects in Figure 3 follow a trend of increasing  $\text{Fe}^+/\text{H}^+ + \text{Fe}^{++}/\text{H}^+$  for decreasing degree of ionization. This trend reflects that for lower ionization objects  $\text{Fe}^{++}$  becomes more important in the total Fe abundance.

### 5. TOTAL ABUNDANCES

We calculate the total oxygen and iron abundances as  $\text{O}/\text{H} = (\text{O}^+/\text{H}^+ + \text{O}^{++}/\text{H}^+) \times \text{ICF}(\text{O})$  and  $\text{Fe}/\text{H} =$

<sup>2</sup> <http://physics.nist.gov/>

TABLE 5  
TOTAL ABUNDANCES FOR THE SAMPLE OF  
H II REGIONS:  $\{X\} = 12 + \log(X/H)$

Object	$\{\text{Fe}\}^a$	$\{\text{Fe}\}^b$	Ref.
M8	$5.69^{+0.12}_{-0.23}$	$5.62^{+0.11}_{-0.21}$	1
M16	$5.16^{+0.12}_{-0.23}$	$5.20^{+0.11}_{-0.19}$	2
M17	$5.82^{+0.12}_{-0.23}$	$5.62^{+0.15}_{-0.32}$	1
M20	$5.31^{+0.12}_{-0.24}$	$5.31^{+0.15}_{-0.21}$	2
M42	$6.02^{+0.12}_{-0.23}$	$5.78^{+0.15}_{-0.33}$	3
M43	$6.01^{+0.13}_{-0.24}$	$6.03^{+0.12}_{-0.23}$	4
NGC 3576	$5.92^{+0.12}_{-0.22}$	$5.91^{+0.14}_{-0.30}$	5
NGC 3603	$6.14^{+0.13}_{-0.24}$	$5.74^{+0.16}_{-0.36}$	2
NGC 7635	$5.40^{+0.12}_{-0.23}$	$5.43^{+0.11}_{-0.21}$	4
S311	$5.17^{+0.12}_{-0.23}$	$5.05^{+0.12}_{-0.21}$	6

REFERENCES.	—	(1)
García-Rojas et al. (2007),	(2007),	(2)
García-Rojas et al. (2006),	(2006),	(3)
Esteban et al. (2004),	(4) Rodríguez	
(2002),	(5) García-Rojas et al. (2004),	
(6) García-Rojas et al. (2005).		

<sup>a</sup> Derived using the ICF of equation (1).

<sup>b</sup> Derived using the ICF of equations (2) and (3).

$(\text{O}/\text{H}) \times (\text{Fe}^{++}/\text{O}^+) \times \text{ICF}(\text{Fe})$ . The ICFs used for Fe are those from Equations (1) and (2)/(3); the ICF scheme from Kingsburgh & Barlow (1994) has been adopted for O:

$$\text{ICF}(\text{O}) = \left( \frac{\text{He}^+ + \text{He}^{++}}{\text{He}^+} \right)^{2/3}. \quad (4)$$

Column 6 in Table 4 shows the values of  $\text{ICF}(\text{O})$  for each PN of the sample. This ICF accounts for the contribution of ions of higher degree of ionization than  $\text{O}^{++}$ , and its value is  $\sim 1.0$  for most of our low-ionization PNe and for the H II regions. The largest values are 1.18 and 1.23 for NGC 3242 and NGC 2392, respectively, the sample PNe with the highest values of  $I(\text{He II } \lambda 4686)/I(\text{H}\beta)$ , 0.26 and 0.33, respectively. The low abundance of  $\text{O}^{+3}$  is confirmed for some of the PNe (IC 3568, NGC 40, NGC 6720, and NGC 6884), where the  $\text{O}^{+3}$  abundances calculated by Liu et al. (2004a) using the  $[\text{O IV}]$  line at  $25.9 \mu\text{m}$ , contribute less than 10% to the total abundances (in fact, these PNe were among the ones we used to define the criteria for the sample selection – see Section 2). Column 7 in Table 4 shows the final values of the O abundances for the sample PNe. Our values of the total O abundances are in reasonable agreement with previous values in the literature. The highest discrepancies are found for Cn 3-1 and NGC 2392. The value of the O abundance in NGC 2392 ranges from  $12 + \log(\text{O}/\text{H}) = 8.35$  to  $8.61$  according to different authors (Barker 1991; Henry et al. 2000; Pottasch et al. 2008), and we find  $12 + \log(\text{O}/\text{H}) = 8.25$ . For Cn 3-1, the difference of  $\sim 0.2$  dex with the results of Wesson et al. (2005) is due to the higher electron density we used.

The Fe abundances obtained from two of the ICFs presented in Section 1 are shown in Tables 4 and 5 for the sample PNe and the group of H II regions. The first of the listed values is based on the ICF implied by photoionization models; the second is based on the ICF derived

using those objects with measurements of both  $[\text{Fe III}]$  and  $[\text{Fe IV}]$  lines. Lowering the first values by  $\sim 0.3$  dex we get a third value for Fe/H and, as discussed in Section 1, these three values of Fe/H can be used to constrain the real value of the gaseous Fe abundance.

The values of  $\text{Fe}^{++}/\text{Fe}$  are very low for the high excitation objects, with the lowest value found for IC 3568, the PNe with the highest degree of ionization in the sample, where  $\text{Fe}^{++}$  contributes less than 10% to the derived Fe abundance. The fact that both  $\text{Fe}^{++}$  and  $\text{O}^+$  have very low abundances in the nebulae with high degrees of ionization suggest that for those objects the real ICFs can show a high dispersion at a given value of  $\text{O}^+/\text{O}^{++}$  (see Figure 2 in Rodríguez & Rubin 2005). This dispersion will translate into errors in the Fe abundances derived from Equations (1) and (2)/(3). Since these are also the objects where Equations (1) and (2) lead to the most discrepant results, their Fe abundances are the less well constrained.

For 11 PNe of the 28 in our sample, there are previous calculations of the Fe abundance, and the differences between our values and the values obtained by other authors go up to 1.7 dex. These differences are due to the use of different atomic data and ICFs. We are using what we think are the best values for all the atomic data (see Rodríguez 2002; Rodríguez & Rubin 2005) and our detailed analysis and the fact that we are using the same procedure for a relatively large sample of objects allow us to compare the results for different objects and to draw some inferences.

Figure 4 shows the values of the Fe abundance derived with the two ICFs from Equations (1) and (2)/(3) as a function of the degree of ionization for all our objects. The axes at the right show the depletion factor,  $[\text{Fe}/\text{H}] = \log(\text{Fe}/\text{H}) - \log(\text{Fe}/\text{H})_{\odot}$ , with  $12 + \log(\text{Fe}/\text{H})_{\odot} = 7.54 \pm 0.03$  (Lodders 2003). It can be seen that all the objects in our sample (both PNe and H II regions) have depletion factors below  $-1.1$  dex. Hence, less than 10% of the solar Fe abundance is present in the gas. If the solar abundance can be considered a good reference for the total Fe abundance (in gas and dust) of these objects (see Section 7), this implies that more than 90% of the Fe atoms are deposited onto dust grains.

The Fe abundances in Figure 4(a) show a trend that suggests that objects with higher degree of ionization have somewhat lower depletion factors. This trend could be related to dust destruction in PNe with harsh radiation fields. However, the trend is not present in Figure 4(b), and if the discrepancy in the Fe abundances implied by Equations (1) and (2) is due to a combination of errors in different atomic data, the depletion factors will be intermediate between the extreme values we are considering, and the trend is likely to disappear.

## 6. PNE WITH HIGH DENSITY AND AGE DEPENDENCE

We have analyzed five additional high-density PNe (see Table 6) because they are likely to be younger than the PNe in our sample, since they have high  $\text{H}\beta$  surface brightness ( $S(\text{H}\beta) > 5 \times 10^{-13} \text{ erg s}^{-1} \text{ cm}^{-2} \text{ arcsec}^{-2}$ ) and high electron densities ( $n_e > 25,000 \text{ cm}^{-3}$ ). To calculate  $S(\text{H}\beta)$  we used the total  $\text{H}\beta$  fluxes and the visual extinction coefficient from Cahn et al. (1992), and the angular sizes from Acker et al. (1992) and Tyllenda et al. (2003). We did not include these objects in the origi-

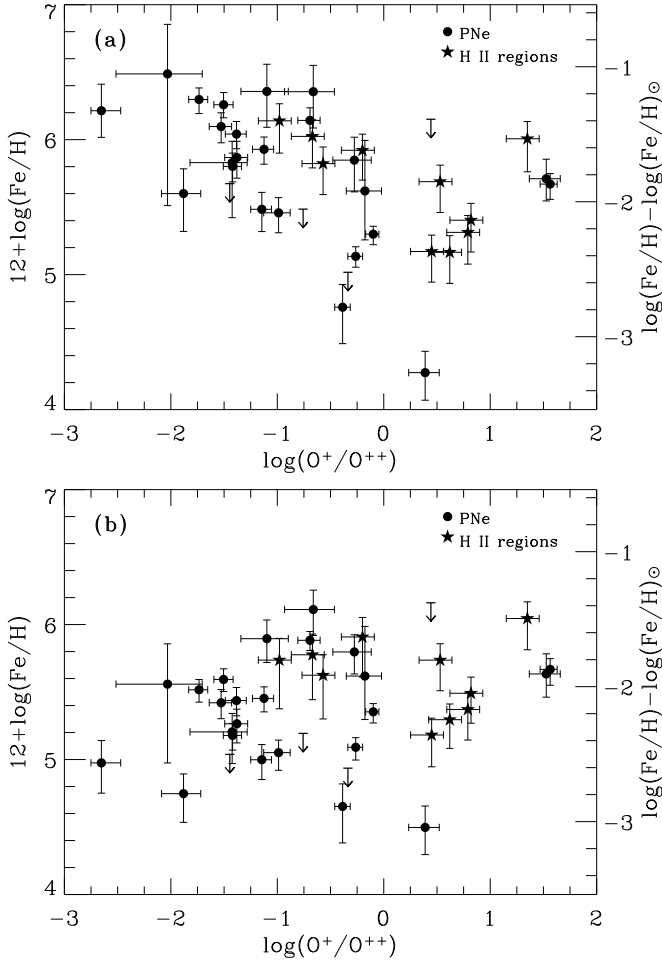


FIG. 4.— Values of Fe/H (left axis) and the depletion factors for Fe/H ( $[\text{Fe}/\text{H}] = \log(\text{Fe}/\text{H}) - \log(\text{Fe}/\text{H})_{\odot}$ , right axis) as a function of the degree of ionization. Panel (a) shows the values obtained from equation (1), and panel (b) is from equations (2)/(3).

nal sample since they show important differences in the values obtained with different diagnostic line ratios (see Table 6), which complicate the calculation of physical conditions and abundances. We decided to constrain the values of the abundances in these PNe by analyzing them in three different ways. The first two rows for the results of each PN in Table 6 show the  $T_e$ 's and ionic abundances derived separately from the two values of  $n_e$  we had for each PN, whereas the third row shows the  $T_e$ 's and ionic abundances obtained by assuming that there is a density gradient in each object and considering different values of  $n_e$  for each ion according to their ionization potential. The differences in the Fe abundances obtained with these three procedures go up to 0.9 dex, and this gives us an idea of the uncertainties involved.

The depletion factors of these five PNe are similar to the values found for the original sample of 28 PNe, with more than 87% of their Fe atoms deposited onto dust grains. We do not find any significant correlation between our derived Fe abundances and  $S(\text{H}\beta)$  (or  $n_e$ ) in the whole group of 33 PNe, which includes objects that are likely to be old such as JnEr 1 or NGC 3587, with

$S(\text{H}\beta) = 8.3 \times 10^{-17}$  and  $1.9 \times 10^{-15}$   $\text{erg s}^{-1} \text{cm}^{-2} \text{arcsec}^{-2}$ , respectively, or objects that are likely to be young, like MyCn 18 with  $S(\text{H}\beta) = 4.4 \times 10^{-11}$   $\text{erg s}^{-1} \text{cm}^{-2} \text{arcsec}^{-2}$  and the high-density objects. The low Fe abundances of our sample PNe and the lack of correlation of the Fe abundances with parameters that can be related to the ages of the objects suggest that no significant destruction of refractory dust grains has taken place in these objects, in agreement with the results found by Stasińska & Szczerba (1999). However, our sample objects are relatively bright PNe, where weak lines have been measured. Hence, we must be missing in our sample the oldest PNe, characterized by low densities, low surface brightness, and large nebular radii. In principle, these old objects could show some evidence for dust destruction.

## 7. DISCUSSION

The O abundances for the original sample of 28 PNe and for the whole sample of 33 PNe are in the ranges 8.25–8.81 and 8.23–8.95 respectively, whereas for the H II regions the range is 8.39–8.56. The dispersion is much higher for the sample PNe, and it can be due to (1) the production or destruction of oxygen in the progenitors of the PNe, or (2) different chemical compositions of the clouds where the central stars formed. In the latter case, different values of Fe/H should be used as the reference abundance to determine depletions.

Both models and observations indicate that oxygen can be produced or destroyed in low-metallicity PNe (i.e., for Magellanic Clouds metallicities, see, e.g., Karakas 2003; Marigo et al. 2003; Leisy & Dennefeld 2006; Karakas et al. 2008), but the standard theoretical results do not predict any significant change in the oxygen abundance at higher metallicities (Marigo et al. 2003; Karakas & Lattanzio 2003; Karakas et al. 2008). However, several authors do not consider this a settled issue (see Perinotto & Corradi 1998; Pottasch & Bernard-Salas 2006; Karakas et al. 2008) and in principle, the O abundances of our sample PNe could still be affected by these effects.

On the other hand, if the dispersion in the O abundances (or part of it) were due to the different initial compositions of the central stars, the Fe/O ratio, that changes slowly with metallicity, would be better suited than Fe/H to derive depletion factors. However, the Fe/O ratio would need a correction for the depletion of oxygen in dust grains. A dust-phase oxygen abundance of 180 parts per million (Cardelli et al. 1996) represents 30% of the solar abundance ( $12 + \log(\text{O}/\text{H})_{\odot} = 8.76$  Lodders (2003)). Assuming that this 30% also applies to our sample PNe, and using the solar value of Fe/O,  $\log(\text{Fe}/\text{O})_{\odot} = -1.22$  (Lodders 2003), the depletion factors implied by Fe/O and Fe/H are similar: the ranges that take into account all the possible values go from  $-3.6$  to  $-0.8$  for  $\log(\text{Fe}/\text{O})$ , and from  $-3.6$  to  $-1.1$  for  $\log(\text{Fe}/\text{H})$ .

Some H-poor central stars of PNe show an iron deficiency of up to  $\sim 1$ –2 dex, which has been associated with  $s$ -process nucleosynthesis occurring in the intershell during the AGB or post-AGB phase (Miksa et al. 2002; Werner et al. 2003; Werner & Herwig 2006; Karakas et al. 2008, and references therein). In these PNe with H-poor central stars some Fe could be

TABLE 6  
 PHYSICAL CONDITIONS, IONIC AND TOTAL ABUNDANCES OF HIGH DENSITY PNE.  $\{X^{+i}\} = 12 + \log(X^{+i}/H^+)$ ,  $\{X\} = 12 + \log(X/H)$

$n_e$ ( $\text{cm}^{-3}$ )	$T_e(\text{[N II]})$ (K)	$T_e(\text{[O III]})$ (K)	$\{\text{He}^+\}$	$\{\text{He}^{++}\}$	$\{\text{O}^+\}$	$\{\text{O}^{++}\}$	ICF	$\{\text{O}\}$	$\{\text{Fe}^{++}\}$	$N^a$	$\{\text{Fe}\}^b$	$\{\text{Fe}\}^c$
M 1-74 (052.2-04.0 <sup>d</sup> )												
$n_e[\text{S II}] = 22300$	12100	9800	11.00	8.07	7.23	8.56	1.00	8.58	5.27	3	6.47	5.89
$n_e[\text{Ar IV}] = 78500$	8100	9200	11.03	9.00	8.48	8.70	1.01	8.90	5.82	3	6.18	6.16
$n_e[\text{S II}]$ and $n_e[\text{Ar IV}]$	12100	9200	11.03	9.00	7.23	8.70	1.01	8.71	5.27	3	6.59	5.95
Me 2-2 (100.0-08.7 <sup>d</sup> )												
$n_e[\text{S II}] = 1000$	15000	10900	11.18	8.09	6.33	8.23	1.00	8.23	4.59	3	6.29	5.43
$n_e[\text{Ar IV}] = 34500$	9500	10400	11.17	8.09	7.79	8.31	1.00	8.43	4.95	3	5.51	5.33
$n_e[\text{S II}]$ and $n_e[\text{Ar IV}]$	15000	10400	11.17	8.09	6.33	8.31	1.00	8.32	4.59	3	6.37	5.46
NGC 5315 (309.1-04.3 <sup>d</sup> )												
$n_e[\text{S II}] = 8400$	10800	9200	11.09	7.62	7.57	8.57	1.00	8.61	3.95	3	4.86	4.45
$n_e[\text{Cl III}] = 28600$	8600	8900	11.09	7.62	8.38	8.63	1.00	8.83	4.58	3	4.96	4.92
$n_e[\text{S II}]$ and $n_e[\text{Cl III}]$	10800	8900	11.09	7.62	7.57	8.63	1.00	8.67	3.95	3	4.91	4.47
NGC 6790 (037.8-06.3 <sup>d</sup> )												
$n_e[\text{Cl III}] = 25700$	14800	13000	11.00	9.52	7.64	8.43	1.02	8.50	4.54	6	5.29	4.98
$n_e[\text{Ar IV}] = 139500$	7800	11300	10.99	9.52	8.68	8.60	1.02	8.95	5.41	6	5.64	5.68
$n_e[\text{Cl III}]$ and $n_e[\text{Ar IV}]$	14800	11300	10.99	9.52	7.64	8.60	1.02	8.65	4.54	6	5.43	5.03
NGC 6807 (042.9-06.9 <sup>d</sup> )												
$n_e[\text{S II}] = 15800$	14600	10600	10.35	8.45	6.52	8.55	1.01	8.56	4.74	3	6.56	5.64
$n_e[\text{Ar IV}] = 54600$	9800	10100	10.35	8.45	7.60	8.65	1.01	8.69	5.17	3	6.13	5.69
$n_e[\text{S II}]$ and $n_e[\text{Ar IV}]$	14600	10100	10.36	8.45	6.52	8.65	1.01	8.65	4.74	3	6.65	5.68

REFERENCES. — *Line intensities from:* Wesson et al. (2005) for M 1-74, Me 2-2, and NGC 6807; Tsamis et al. (2003) for NGC 6790; and Liu et al. (2004b) for NGC 5315.

<sup>a</sup> Number of [Fe III] lines used in the Fe<sup>++</sup> abundance determination.

<sup>b</sup> Derived using the ICF of equation (1).

<sup>c</sup> Derived using the ICF of equation (2) and (3).

<sup>d</sup> PNG identifications from Acker et al. (1992).

depleted because of this process, and 13 PNe of our sample have this type of central star: Cn 3-1, IC 1747, IC 5217, JnEr 1, M 1-73, MyCn 18, NGC 40, NGC 5315, NGC 6153, NGC 6543, NGC 6572, NGC 6803, and NGC 7026 (van der Hucht et al. 1981; Liebert et al. 1988; Mendez 1991; Tylenda et al. 1993; Crowther et al. 1998; Parthasarathy et al. 1998; Liu et al. 2000; Bohigas 2001; Lee et al. 2007; Sterling & Dinerstein 2008). However, Sterling & Dinerstein (2008) concluded recently that the compositions of PNe with H-poor central stars are not different from those PNe that have H-rich central stars. Furthermore, we do not see any systematic difference in the Fe abundances derived for PNe with H-rich and H-poor central stars.

The error bars in Figure 4 do not take into account those uncertainties arising from the ICF, and these errors could explain most of the dispersion in Fe/H shown by the high excitation objects. However, some of the dispersion shown by all the PNe is likely to be real and due to different depletion factors, since it is quite high in some cases, with differences in the Fe abundances up to  $\sim 1.5$  dex for those objects with  $\log(\text{O}^+/\text{O}^{++}) \sim -0.5$ . We did not find any obvious difference in the morphology, the type of the central star, or the dust chemistry of the PNe with the highest and lowest depletion factors. Using the C/O values and the infrared dust features identified in the literature, we infer that 13 PNe of the sample are O-rich ( $\text{C}/\text{O} < 1$ ), 8 are C-rich ( $\text{C}/\text{O} > 1$  and/or they show PAHs or SiC in their spectra), and 7 are uncertain since  $\text{C}/\text{O} \sim 1$  or they do not have clear dust features (Cohen et al. 1986; Rola & Stasińska 1994; Roche et al. 1996; Kholtygin 1998; Kwitter & Henry 1998; Pottasch & Beintema 1999; Henry et al. 2000;

Liu et al. 2000; Casassus et al. 2001; Tsamis et al. 2003; Liu et al. 2004a; Pottasch et al. 2004; Tsamis et al. 2004; Cohen & Barlow 2005; Wesson et al. 2005; Smith & McLean 2008). It is not clear yet which are the main iron compounds condensing onto dust grains, but O-rich environments are expected to have metallic iron grains, silicates, and oxides, whereas C-rich environments can have their iron in the form of metallic grains, Fe<sub>3</sub>C, FeSi, FeS, and FeS<sub>2</sub> (Whittet 2003; Ferrarotti & Gail 2006). The fact that we do not see any systematic difference between the Fe abundances of C-rich and O-rich PNe suggests that the iron depletion efficiencies in C-rich and O-rich environments are similar. This is supported by the lack of systematic differences between the iron abundances of PNe with H-rich and H-poor central stars mentioned above, since H-poor central stars are usually C-rich (De Marco & Barlow 2001; Peña et al. 2003).

### 7.1. Dust-to-gas ratios

If we assume that gas and dust evolve together, we can derive a lower limit to the dust-to-gas mass ratio taking into account that at least 90% of the solar Fe abundance is deposited onto dust grains in the objects of our sample. We find that  $M_{\text{dust}}/M_{\text{gas}} \geq 1.3 \times 10^{-3}$ , but elements like Si and Mg can have similar contributions to the mass of dust grains and the contributions of C and O can be even higher (see e.g. Sofia et al. 1994). The dust-to-gas mass ratios derived by Stasińska & Szczerba (1999) are lower than this lower limit by factors up to 17 for 10 PNe of our sample. This illustrates how difficult it is to find a reliable value for the dust-to-gas ratio using infrared dust emission (see also Stasińska & Szczerba 1999;

Górny et al. 2001; Phillips 2007).

## 8. SUMMARY AND CONCLUSIONS

We have constrained the iron abundances in a sample of 33 low-ionization PNe using the ICFs scheme developed by Rodríguez & Rubin (2005). This is the largest sample of PNe where the iron abundance has been calculated, including 18 nebulae with first determinations. The fact that we considered quite drastic changes in the atomic data involved, and the fact that we analyzed the whole sample with the same procedure, allow us to constrain the real value of the Fe abundances and compare the results between objects. The depletion factors ( $[\text{Fe}/\text{H}] = \log(\text{Fe}/\text{H}) - \log(\text{Fe}/\text{H})_{\odot}$ ) of the PNe are below  $-0.9$  dex, which implies that more than  $\sim 90\%$  of the total Fe abundance is condensed onto dust grains. This result suggests that the efficiency with which Fe atoms attach to dust grains is higher than the one predicted by the models of AGB dust production of Ferrarotti & Gail (2006). We derived a lower limit to the dust-to-gas mass ratio for the sample PNe just by considering that 90% of their iron atoms are condensed onto dust grains,  $M_{\text{dust}}/M_{\text{gas}} \geq 1.3 \times 10^{-3}$ . Other elements, such as Si, Mg, C, and O, will have similar or higher contributions to the mass of dust grains.

The derived depletion factors span about two orders of magnitude, but we have not found any significant correlation between the derived Fe abundances and the evolutionary parameters of our sample PNe (surface brightness or electron density), in agreement with the results obtained by Stasińska & Szczerba (1999). This result suggests that no significant destruction of dust grains

is taking place in these objects. The different depletion factors shown by the PNe could be due either to different dust condensation efficiencies or to the destruction of a minor dust component in some objects.

We do not find any systematic difference in the Fe abundances that can be related to the morphology, the type of the central star (i.e., H-rich or H-poor central star), or the dust chemistry. This result suggests that C-rich and O-rich progenitor stars have similar iron depletion efficiencies. However, the lack of identifications of dust features in most of the sample PNe, and the uncertainties associated with the value of the C/O ratio, imply that this issue cannot be considered settled.

We have compared our results with the values derived for a group of 10 H II regions using the same procedure. The high depletion factors found for both kinds of objects imply that the atmospheres of AGB stars deplete refractory elements onto dust grains as efficiently as molecular clouds, whereas dust destruction processes are not very efficient in either H II regions or PNe.

The authors thank Jorge García-Rojas for helpful comments, Roger Wesson for sending some extra measurements of line intensities, and Michael Witthoeft for providing the atomic data for [Fe VII]. We also thank an anonymous referee for helpful comments that improved the paper. This work has made use of NASA's Astrophysics Data System, and the SIMBAD database operated at CDS, Strasbourg, France. GD-I and MR acknowledge support from Mexican CONACYT project 50359-F.

## REFERENCES

- Acker, A., Marcout, J., Ochsenbein, F., Stenholm, B., & Tylenda, R. 1992, Strasbourg - ESO catalogue of galactic planetary nebulae (Garching: European Southern Observatory, 1992)
- Aller, L. H. & Czyzak, S. J. 1983, *ApJS*, 51, 211
- Aller, L. H., Ross, J. E., Omara, B. J., & Keyes, C. D. 1981, *MNRAS*, 197, 95
- Barker, T. 1991, *ApJ*, 371, 217
- Bautista, M. A. & Pradhan, A. K. 1996, *A&AS*, 115, 551
- Beckwith, S., Evans, II, N. J., Natta, A., Russell, R. W., & Wyant, J. 1984, *ApJ*, 277, 207
- Benjamin, R. A., Skillman, E. D., & Smits, D. P. 1999, *ApJ*, 514, 307
- Bohigas, J. 2001, *RevMexAA*, 37, 237
- Cahn, J. H., Kaler, J. B., & Stanghellini, L. 1992, *A&AS*, 94, 399
- Cardelli, J. A., Clayton, G. C., & Mathis, J. S. 1989, *ApJ*, 345, 245
- Cardelli, J. A., Meyer, D. M., Jura, M., & Savage, B. D. 1996, *ApJ*, 467, 334
- Casassus, S., Roche, P. F., Aitken, D. K., & Smith, H. 2001, *MNRAS*, 327, 744
- Casassus, S., Roche, P. F., & Barlow, M. J. 2000, *MNRAS*, 314, 657
- Chen, G. X., & Pradhan, A. K. 1999, *A&AS*, 136, 395
- Chen, G. X., & Pradhan, A. K. 2000, *A&AS*, 147, 111
- Clegg, R. E. S., Harrington, J. P., Barlow, M. J., & Walsh, J. R. 1987a, *ApJ*, 314, 551
- Clegg, R. E. S., Peimbert, M., & Torres-Peimbert, S. 1987b, *MNRAS*, 224, 761
- Cohen, M., Allamandola, L., Tielens, A. G. G. M., Bregman, J., Simpson, J. P., Witteborn, F. C., Wooden, D., & Rank, D. 1986, *ApJ*, 302, 737
- Cohen, M., & Barlow, M. J. 2005, *MNRAS*, 362, 1199
- Crowther, P. A., De Marco, O., & Barlow, M. J. 1998, *MNRAS*, 296, 367
- De Marco, O., & Barlow, M. J. 2001, *Ap&SS*, 275, 53
- Esteban, C., Peimbert, M., García-Rojas, J., Ruiz, M. T., Peimbert, A., & Rodríguez, M. 2004, *MNRAS*, 355, 229
- Ferrarotti, A. S. & Gail, H.-P. 2006, *A&A*, 447, 553
- García-Rojas, J., Esteban, C., Peimbert, A., Peimbert, M., Rodríguez, M., & Ruiz, M. T. 2005, *MNRAS*, 362, 301
- García-Rojas, J., Esteban, C., Peimbert, A., Rodríguez, M., Peimbert, M., & Ruiz, M. T. 2007, *RevMexAA*, 43, 3
- García-Rojas, J., Esteban, C., Peimbert, M., Costado, M. T., Rodríguez, M., Peimbert, A., & Ruiz, M. T. 2006, *MNRAS*, 368, 253
- García-Rojas, J., Esteban, C., Peimbert, M., Rodríguez, M., Ruiz, M. T., & Peimbert, A. 2004, *ApJS*, 153, 501
- Garstang, R. H., Robb, W. D., & Rountree, S. P. 1978, *ApJ*, 222, 384
- Georgiev, L. N., Richer, M. G., Arrieta, A., & Zhekov, S. A. 2006, *ApJ*, 639, 185
- Górny, S. K., Stasińska, G., Szczerba, R., & Tylenda, R. 2001, *A&A*, 377, 1007
- Henry, R. B. C., Kwitter, K. B., & Bates, J. A. 2000, *ApJ*, 531, 928
- Hyung, S., Aller, L. H., Feibelman, W. A., & Lee, W.-B. 2001a, *AJ*, 122, 954
- Hyung, S., Aller, L. H., & Lee, W.-B. 2001b, *PASP*, 113, 1559
- Karakas, A. I., 2003, Thesis, Monash University, Melbourne
- Karakas, A. I., & Lattanzio, J. C. 2003, *Publ. Astron. Soc. Australia*, 20, 393
- Karakas, A. I., van Raai, M. A., Lugaro, M., Sterling, N. C., & Dinerstein, H. L. 2008, *ApJ*, 690, 1130
- Keenan, F. P., & Norrington, P. H. 1987, *A&A*, 181, 370
- Keyes, C. D., Aller, L. H., & Feibelman, W. A. 1990, *PASP*, 102, 59
- Kholytgin, A. F. 1998, *A&A*, 329, 691
- Kingdon, J., Ferland, G. J., & Feibelman, W. A. 1995, *ApJ*, 439, 793
- Kingsburgh, R. L. & Barlow, M. J. 1994, *MNRAS*, 271, 257

- Kwitter, K. B., & Henry, R. B. C. 1998, *ApJ*, 493, 247
- Lee, T.-H., Stanghellini, L., Ferrario, L., & Wickramasinghe, D. T. 2007, in *ASP Conf. Ser.* 372, 15th European Workshop on White Dwarfs, ed. R. Napiwotzski & M. R. Burleigh, (San Francisco: ASP), 173
- Leisy, P., & Dennefeld, M. 2006, *A&A*, 456, 451
- Lenzuni, P., Natta, A., & Panagia, N. 1989, *ApJ*, 345, 306
- Liebert, J., Fleming, T. A., Green, R. F., & Grauer, A. D. 1988, *PASP*, 100, 187
- Likkell, L., Dinerstein, H. L., Lester, D. F., Kindt, A., & Bartig, K. 2006, *AJ*, 131, 1515
- Liu, Y., Liu, X.-W., Barlow, M. J., & Luo, S.-G. 2004a, *MNRAS*, 353, 1251
- Liu, Y., Liu, X.-W., Luo, S.-G., & Barlow, M. J. 2004b, *MNRAS*, 353, 1231
- Liu, X.-W., Storey, P. J., Barlow, M. J., Danziger, I. J., Cohen, M., & Bryce, M. 2000, *MNRAS*, 312, 585
- Lodders, K. 2003, *ApJ*, 591, 1220
- Lucy, L. B. 1995, *A&A*, 294, 555
- Marigo, P., Bernard-Salas, J., Pottasch, S. R., Tielens, A. G. G. M., & Wesselius, P. R. 2003, *A&A*, 409, 619
- Méndez, R. H. 1991, in *IAU Symp.* 145, *The Photospheric Abundance Connection*, ed. G. Michaud & A. Tutukov (Dordrecht: Kluwer), 375
- Mendoza, C. 1983, in *IAU Symp.* 103, *Planetary Nebulae*, ed. D. R. Flower (Dordrecht: Riedel), 143
- Mendoza, C., & Zeppen, C. J. 1982, *MNRAS*, 198, 127
- Middlemass, D. 1990, *MNRAS*, 244, 294
- Miksa, S., Deetjen, J. L., Dreizler, S., Kruk, J. W., Rauch, T., & Werner, K. 2002, *A&A*, 389, 953
- Morton, D. C. 1974, *ApJ*, 193, L35
- Morton, D. C., Drake, J. F., Jenkins, E. B., Rogerson, J. B., Spitzer, L., & York, D. G. 1973, *ApJ*, 181, L103
- Nussbaumer, H., & Storey, P. J. 1978, *A&A*, 70, 37
- Nussbaumer, H., Storey, P. J., & Storey, P. J. 1982, *A&A*, 113, 21
- Osterbrock, D. E., & Ferland, G. J. 2006, *Astrophysics of gaseous nebulae and active galactic nuclei* (2nd. ed.; Sausalito, CA: University Science Books)
- Parthasarathy, M., Acker, A., & Stenholm, B. 1998, *A&A*, 329, L9
- Peimbert, A., & Peimbert, M. 2005, *RevMexAA Conf. Ser.*, 23, 9
- Peña, M., Medina, S., & Stasińska, G. 2003, *RevMexAA*, 18, 84
- Péquignot, D., & Stasińska, G. 1980, *A&A*, 81, 121
- Pérez-Montero, E., & Díaz, A. I. 2003, *MNRAS*, 346, 105
- Perinotto, M., Bencini, C. G., Pasquali, A., Machado, A., Rodríguez Espinosa, J. M., & Stanga, R. 1999, *A&A*, 347, 967
- Perinotto, M., & Corradi, R. L. M. 1998, *A&A*, 332, 721
- Phillips, J. P. 2007, *MNRAS*, 381, 117
- Pottasch, S. R., Baud, B., Beintema, D., Emerson, J., Harris, S., Habing, H. J., Houck, J., Jennings, R., & Marsden, P. 1984, *A&A*, 138, 10
- Pottasch, S. R. & Beintema, D. A. 1999, *A&A*, 347, 975
- Pottasch, S. R., Beintema, D. A., Bernard Salas, J., & Feibelman, W. A. 2001, *A&A*, 380, 684
- Pottasch, S. R., Beintema, D. A., Bernard Salas, J., Koornneef, J., & Feibelman, W. A. 2002, *A&A*, 393, 285
- Pottasch, S. R., & Bernard-Salas, J. 2006, *A&A*, 457, 189
- Pottasch, S. R., Bernard-Salas, J., Beintema, D. A., & Feibelman, W. A. 2003, *A&A*, 409, 599
- Pottasch, S. R., Bernard-Salas, J., Beintema, D. A., & Feibelman, W. A. 2004, *A&A*, 423, 593
- Pottasch, S. R., Bernard-Salas, J., & Roellig, T. L. 2007, *A&A*, 471, 865
- Pottasch, S. R., Bernard-Salas, J., & Roellig, T. L. 2008, *A&A*, 481, 393
- Pottasch, S. R. & Surendiranath, R. 2005, *A&A*, 444, 861
- Pottasch, S. R., & Surendiranath, R. 2007, *A&A*, 462, 179
- Pwa, T. H., Pottasch, S. R., & Mo, J. E. 1986, *A&A*, 164, 184
- Quinet, P. 1996, *A&AS*, 116, 573
- Roche, P. F., Lucas, P. W., Hoare, M. G., Aitken, D. K., & Smith, C. H. 1996, *MNRAS*, 280, 924
- Rodríguez, M. 1996, *A&A*, 313, L5
- . 2002, *A&A*, 389, 556
- . 2003, *ApJ*, 590, 296
- Rodríguez, M. & Rubin, R. H. 2005, *ApJ*, 626, 900
- Rola, C., & Stasińska, G. 1994, *A&A*, 282, 199
- Sharpee, B., Williams, R., Baldwin, J. A., & van Hoof, P. A. M. 2003, *ApJS*, 149, 157
- Shields, G. A. 1975, *ApJ*, 195, 475
- . 1978, *ApJ*, 219, 559
- Shields, G. A., Aller, L. H., Keyes, C. D., & Czyzak, S. J. 1981, *ApJ*, 248, 569
- Smith, E. C. D., & McLean, I. S. 2008, *ApJ*, 676, 408
- Sofia, U. J., Cardelli, J. A., & Savage, B. D. 1994, *ApJ*, 430, 650
- Stasińska, G. & Szczerba, R. 1999, *A&A*, 352, 297
- Sterling, N. C., & Dinerstein, H. L. 2008, *ApJS*, 174, 158
- Sterling, N. C., Dinerstein, H. L., Bowers, C. W., & Redfield, S. 2005, *ApJ*, 625, 368
- Storey, P. J., & Hummer, D. G. 1995, *MNRAS*, 272, 41
- Sugar, J., & Corliss, C. 1985, *J. Phys. Chem. Ref. Data*, 14, 1
- Tsamis, Y. G., Barlow, M. J., Liu, X.-W., Danziger, I. J., & Storey, P. J. 2003, *MNRAS*, 345, 186
- Tsamis, Y. G., Barlow, M. J., Liu, X.-W., Storey, P. J., & Danziger, I. J. 2004, *MNRAS*, 353, 953
- Tylenda, R., Acker, A., & Stenholm, B. 1993, *A&AS*, 102, 595
- Tylenda, R., Siódmiak, N., Górny, S. K., Corradi, R. L. M., & Schwarz, H. E. 2003, *A&A*, 405, 627
- van der Hucht, K. A., Conti, P. S., Lundstrom, I., & Stenholm, B. 1981, *Space Science Reviews*, 28, 227
- Werner, K., Deetjen, J. L., Dreizler, S., Rauch, T., & Kruk, J. W. 2003, in *IAU Symp.* 209, *Planetary Nebulae: Their Evolution and Role in the Universe*, ed. S. Kwok, M. Dopita, & R. Sutherland (San Francisco: ASP), 169
- Werner, K., & Herwig, F. 2006, *PASP*, 118, 183
- Wesson, R. & Liu, X.-W. 2004, *MNRAS*, 351, 1026
- Wesson, R., Liu, X.-W., & Barlow, M. J. 2005, *MNRAS*, 362, 424
- Witthoef, M. C., & Badnell, N. R. 2008, *A&A*, 481, 543
- Whittet, D. C. B. 2003, *Dust in the galactic environment* (2nd ed.; Bristol: IoP)
- Zhang, H. 1996, *A&AS*, 119, 523